Evolution of El Niño–Southern Oscillation and global atmospheric surface temperatures

Kevin E. Trenberth, Julie M. Caron, David P. Stepaniak, and Steve Worley

National Center for Atmospheric Research, Boulder, Colorado, USA

[1]   The origins of the delayed increases in global surface temperature accompanying El Niño events and the implications for the role of diabatic processes in El Niño–Southern Oscillation (ENSO) are explored. The evolution of global mean surface temperatures, zonal means and fields of sea surface temperatures, land surface temperatures, precipitation, outgoing longwave radiation, vertically integrated diabatic heating and divergence of atmospheric energy transports, and ocean heat content in the Pacific is documented using correlation and regression analysis. For 1950–1998, ENSO linearly accounts for 0.06°C of global surface temperature increase. Warming events peak 3 months after SSTs in the Niño 3.4 region, somewhat less than is found in previous studies. Warming at the surface progressively extends to about ±30° latitude with lags of several months. While the development of ocean heat content anomalies resembles that of the delayed oscillator paradigm, the damping of anomalies through heat fluxes into the atmosphere introduces a substantial diabatic component to the discharge and recharge of the ocean heat content. However, most of the delayed warming outside of the tropical Pacific comes from persistent changes in atmospheric circulation forced from the tropical Pacific. A major part of the ocean heat loss to the atmosphere is through evaporation and thus is realized in the atmosphere as latent heating in precipitation, which drives teleconnections. Reduced precipitation and increased solar radiation in Australia, Southeast Asia, parts of Africa, and northern South America contribute to surface warming that peaks several months after the El Niño event. Teleconnections contribute to the extensive warming over Alaska and western Canada through a deeper Aleutian low and stronger southerly flow into these regions 0–12 months later. The 1976/1977 climate shift and the effects of two major volcanic eruptions in the past 2 decades are reflected in different evolution of ENSO events. At the surface, for 1979–1998 the warming in the central equatorial Pacific develops from the west and progresses eastward, while for 1950–1978 the anomalous warming begins along the coast of South America and spreads westward. The eastern Pacific south of the equator warms 4–8 months later for 1979–1998 but cools from 1950 to 1978.   *INDEX TERMS:* 1620 Global Change: Climate dynamics (3309); 4215 Oceanography: General: Climate and interannual variability (3309); 4522 Oceanography: Physical: El Niño; 3339 Meteorology and Atmospheric Dynamics: Ocean/atmosphere interactions (0312, 4504); *KEYWORDS:* global temperatures, ENSO, delayed oscillator, teleconnections, climate change, sea surface temperatures

1.   Introduction

[2]   Following an El Niño the global surface air temperature typically warms up by perhaps 0.1°C with a lag of ∼6 months [*Newell and Weare*, 1976; *Pan and Oort*, 1983; *Jones*, 1989; *Wigley*, 2000]. In an exceptional event such as the 1997–1998 El Niño the amount exceeds 0.2°C. *Christy and McNider* [1994] and *Angell* [2000] show that the entire troposphere warms up with an overall lag of 5–6 months, but the lag is slightly less in the tropics and is greater at higher latitudes. Consequently, the empirical evidence suggests a strong diabatic component to El Niño–Southern Oscillation (ENSO).

[3]   However, several theories of ENSO involve an exchange of heat in the equatorial Pacific Ocean with other parts of the ocean and thus are largely adiabatic. In particular, theories of El Niño based on the delayed oscillator paradigm for ENSO [*Suarez and Schopf*, 1988; *Jin*, 1997] and the Cane-Zebiak model [*Cane and Zebiak*, 1985] move heat out of the equatorial region during El Niño but move heat back as part of the overall ENSO cycle. It has

been suggested that the timescale of ENSO is determined by the time required for an accumulation of warm water in the tropics to essentially recharge the system plus the time for the El Niño itself to evolve [*Wyrtki*, 1985]. The amount of warm water in the tropical Pacific builds up prior to and is then depleted during ENSO [*Cane and Zebiak*, 1985; *Jin*, 1997; *Tourre and White*, 1995; *Giese and Carton*, 1999; *Meinen and McPhaden*, 2000]. Observed changes in subsurface ocean temperatures [*Zhang and Levitus*, 1996, 1997] and sea level [*Smith*, 2000] and how they evolve with ENSO provide further support. Nevertheless, it has not been clear from observations how much of the heat content change is from diabatic effects.

[4]   Therefore a key issue is the extent of the role of diabatic processes in ENSO and how the increase in global mean temperatures comes about. Previous studies that have investigated a link between global mean temperatures and ENSO have not dealt with the spatial structure that exists, except for a case study of the 1997/1998 El Niño event by *Kumar et al.* [2001]. Progress on these questions may also help determine the role of ENSO in the global climate system. We will show that much of the ocean heat content buildup and depletion is through diabatic exchanges of heat with the atmosphere. One possible mechanism is that the

atmospheric circulation and cloudiness change with ENSO in such a way as to produce a warming primarily from processes directly within the atmosphere. Another possibility is that following El Niño the ocean gives up heat to the atmosphere to produce the delayed warming. In fact, both seem to occur. The latter appears to be more likely in the tropics and subtropics and was confirmed for a limited period by *Sun and Trenberth* [1998] and *Sun* [2000]. However, in the extratropics of the Northern Hemisphere the deeper Aleutian low that accompanies El Niño advects warm moist air along the west coast of North America, bringing warmth to western Canada and Alaska [*Trenberth and Hurrell*, 1994]. Similarly, in most parts of the tropics, through teleconnections and because the main precipitation shifts to the central Pacific, drier and sunnier conditions favor higher temperatures with El Niño [*Klein et al.*, 1999]. These examples suggest that several mechanisms play a role in the mini global warming following El Niño. Hence a primary purpose of this paper is to clarify how the global atmospheric surface temperatures respond to ENSO through changes in the heat budget.

[5] In the work by *Halpert and Ropelewski* [1992], and several earlier articles by the same authors, they have documented land surface temperature linkages with the Southern Oscillation as composites for an idealized 24-month sequence from July before to June after the ENSO events. They state that [*Halpert and Ropelewski*, 1992, p. 590] "The general increase or decrease in surface temperatures throughout the global tropics is a delayed response to the warming or cooling of the equatorial SSTs, primarily in the Pacific." However, they do not document how this comes about, although they suggest that variations in cloud cover are important in Africa and Southeast Asia, and they discuss the likely role of teleconnections in the extratropics. They further point out, but do not explore, the need to relate ENSO to global mean temperatures by not using calendar year means, owing to the propensity for ENSO events to peak at the end of the year. All of these aspects are addressed in this study.

[6] Sea surface temperatures (SSTs) are a key in the two-way communication between the atmosphere and ocean but have to be supported by a substantial heat content anomaly of the ocean mixed layer if they are to have a continuing influence on the atmosphere. Such an influence typically means that the anomalous heat is being drained from the ocean and thus a negative feedback occurs, as seems to be the case generally in the tropics. This was shown from computations using observations by *Trenberth et al.* [2002], who demonstrated how the coupled atmosphere and ocean respond to ENSO via a singular value decomposition (SVD) analysis of the temporal covariance of SST with the divergence of the vertically integrated energy transports in the atmosphere, precipitation, atmospheric diabatic heating, and other fields. The first two coupled modes, explaining 39.5% and 15.4% of the covariance, featured different aspects of ENSO that are related at several-seasons lag. The time series of the first coupled mode is well depicted by that of the SSTs in the tropical central and eastern Pacific, represented by SST anomalies in the Niño 3.4 region ($170°W–120°W$, $5°N–5°S$), referred to as N3.4. The second mode is depicted by the contrast in SST differences across the Pacific from about the dateline to coastal South America and can be represented by the normalized difference in SSTs in Niño regions 1 and 2 ($0–10°S$, $90°W–80°W$) (hereinafter referred to as Niño $1 + 2$) minus Niño 4 ($5°N–5°S$, $160°E–150°W$), called the Trans-Niño Index (TNI) [*Trenberth and Stepaniak*, 2001]. The study showed that in the tropical Pacific during major El Niño events, the anomalies in divergence of the atmospheric energy transports exceed 50 W m^{-2} over broad regions and primarily come from surface fluxes from the ocean to the atmosphere. High SSTs associated with warm ENSO events are damped through surface heat fluxes into the atmosphere which fuel teleconnections and atmospheric circulation changes that transport the energy into

higher latitudes and throughout the tropics, contributing to loss of heat by the ocean. Cold ENSO events correspond to a recharge phase as heat enters the ocean. The evolution of ENSO and the lag relationships manifested between the N3.4 and TNI indices [*Trenberth et al.*, 2002; *Trenberth and Stepaniak*, 2001] suggests that a systematic exploration of lead and lag relationships in the evolution of ENSO is warranted and that the N3.4 index can be used as the key index. Hence these aspects are the focus of this paper.

[7] An important factor to be recognized in the evolution of SST patterns with ENSO and its changes over time is the 1976–1977 climate shift of ENSO activity toward more warm phases after about 1976 [*Trenberth*, 1990], which is very unusual given the record of the previous 100 years [*Trenberth and Hoar*, 1996, 1997; *Urban et al.*, 2000], and has been linked to decadal changes in climate throughout the Pacific basin and to changes in evolution of ENSO [*Trenberth and Hurrell*, 1994; *Graham*, 1994; *Trenberth and Stepaniak*, 2001]. The issue of the statistical significance of the 1976–1977 shift has been raised by *Wunsch* [1999] and *Rajagopalan et al.* [1997], although their statistical models have been challenged by *Trenberth and Hurrell* [1999a, 1999b]. *Rasmusson and Carpenter* [1982] presented composites of the evolution of ENSO events for six warm ENSO events from 1951 to 1972 and showed the "antecedent," "onset," "peak," "transition," and "mature" phases of the composite event. These run from September of the year before to January of the year following the event and became known as the "canonical" El Niño; see *Wallace et al.* [1998] for a historical perspective. Before 1976, ENSO events began along the west coast of South America and developed westward. In contrast, after 1977 the warming developed from the west, so that the evolution of ENSO events changed abruptly about 1976/1977 [*Wang*, 1995; *An and Wang*, 2000; *Trenberth and Stepaniak*, 2001].

[8] In addition to the climate shift, the more recent period may be anomalous in ENSO evolution and its effects on surface temperatures owing to the presence of two strong volcanic eruptions (El Chichon in April 1982 and Pinatubo in June 1991). *Wigley* [2000] estimates a global mean cooling from the two volcanoes peaking at $-0.2°C$ for El Chichon and at $-0.5°C$ for Pinatubo some 13 months after the eruption. Several of our data sets, especially those dependent on satellite information, begin in 1979. Accordingly, we provide the most complete analysis for the post-1979 period. We take 1979–1998 as representative of the post-1976/1977 period. However, we also wish to know the extent to which our results apply more generally in previous periods. Hence we also explore the relationships for the 1950–1978 interval whenever adequate data are available in order to examine the reproducibility of the results and impacts of the 1976/1977 shift and volcanic influences.

[9] We exploit several new data sets, described in section 2, to help deduce and clarify what can be said about the diabatic processes involved in ENSO, how they relate to SST variations and the heat content of the subsurface ocean, and how the mini global warming following El Niño arises when it appears that it cannot be sustained by the atmosphere alone. Tropical precipitation variations are explored as a key indicator of the latent heating of the atmosphere, and inferences are made about effects of changes in cloudiness and increased solar radiation and about surface wetness on sensible versus latent heating. The presentation of results in section 3 proceeds from the relationships between ENSO and global mean temperature, to zonal means of various quantities, and subsequently to full geographic spatial structure, so that we can trace the origin of the relationships. Results for 1950–1978 are presented along with those for 1979–1998 where available. In discussing the results in section 4, the relative roles of the links of global temperatures with ENSO via the Pacific Ocean and via teleconnections through the atmosphere are addressed. The conclusions are given in section 5.

2. Data and Methods

[10] Most of the in-depth analysis here is for the period 1979–1998, as this is the time when high-quality atmospheric reanalyses are available from the National Centers for Environmental Prediction/National Center for Atmospheric Research (NCEP/NCAR). In addition, global fields of precipitation and outgoing longwave radiation (OLR) are also available for this period. Prior to 1979 the absence of satellite data adversely affects the quality of the reanalyses. For the period 1979–1998 we computed many quantities for each month, including the vertically integrated total atmospheric energy transports $\mathbf{F_A}$, their divergence $\nabla \cdot \mathbf{F_A}$, and the vertically integrated diabatic heating [*Trenberth et al.*, 2001]. The total energy consists of the potential, internal, latent, and kinetic energy, while the transports of the total energy include a pressure-work term and can be broken down into components from the dry static energy and the latent energy, which together make up the moist static energy, plus the kinetic energy. The energy tendencies are combined with the computed divergence of the vertically integrated atmospheric energy transports to give the net column change, which has to be balanced by the top-of-the-atmosphere (TOA) radiation and/or the surface fluxes; see *Trenberth and Solomon* [1994] and *Trenberth et al.* [2001] for details. In practice, the tendency terms average to be very small over a few months, and neglecting them gives

$$\nabla \cdot \mathbf{F_A} = R_T + F_s, \qquad (1)$$

where R_T is the net downward top-of-atmosphere radiation and F_s is the upward surface flux. The diabatic heating is sometimes called Q_1, and, ignoring a tiny frictional heating component (Q_f), in vertically integrated form, is given by

$$Q_1 = R_T + F_s + L(P - E), \qquad (2)$$

where P is the precipitation and E is the evaporation in the column and L is the latent heat of vaporization. The term LE cancels a part of F_s, leaving the surface radiation and sensible heat flux terms. Precipitation simply increases the dry static energy at the expense of the moisture content as the convergence of moisture in the low levels is realized as latent heating. Hence there is a strong compensation between the dry and moist components of moist static energy, and Q_1 is not directly related.

[11] *Trenberth et al.* [2001] show that the variability of TOA fluxes is small and so $\nabla \cdot \mathbf{F_A}$ is mainly balanced by the surface fluxes. *Trenberth et al.* [2002] exploit the large spatial and temporal scales of ENSO to bring out the ENSO signal from the noise. Over the Niño 3.4 region, results imply a random standard error of ~6 W m^{-2} and suggest that signals of >12 W m^{-2} are significant.

[12] We also make use of the OLR data set from the National Oceanic and Atmospheric Administration (NOAA) series of satellites adjusted using results from *Waliser and Zhou* [1997], as given by *Trenberth et al.* [2002]. We utilize the precipitation data set from *Xie and Arkin* [1996, 1997], called the Climate Prediction Center (CPC) Merged Analysis of Precipitation (CMAP). Over land, precipitation is mainly based on information from rain gauge observations, while over the ocean, use is primarily made of satellite estimates from several different algorithms based on OLR and scattering and emission of microwave radiation.

[13] We use the NCEP SSTs from the optimal interpolation SST analysis of *Reynolds and Smith* [1994] after 1982 and the empirical orthogonal function reconstructed SST analysis of *Smith et al.* [1996] for the period before then. The latter does not contain anomalies south of 40°S. However, these SSTs are preferred to those in the global surface temperature data set from the University of East Anglia (UEA) and the United Kingdom Meteorological Office [*Hurrell and Trenberth*, 1999], although the latter is

employed to examine values over land and to examine the longer record and the global means.

[14] To examine aspects of the subsurface ocean heat content changes, we have used the ocean analyses of the tropical Pacific from the Environmental Modeling Center at NCEP. These model-based analyses have developed over time and currently assimilate observed surface and subsurface ocean temperatures, as well as satellite altimetry sea level data from TOPEX/Poseidon. We use a monthly mean analysis from 1980 to 1998 derived from weekly analyses using the RA6 schemes described by *Behringer et al.* [1998].

[15] The RA6 wind forcing and surface heat flux have changed over time. For 1980–1996 the wind forcing used was the *Hellerman and Rosenstein* [1983] climatological wind stress combined with monthly pseudostress fields from Florida State University. NCEP operational near-surface winds, four times daily, with a constant drag coefficient, were used to determine wind stress for 1997 through mid-1998. From mid-1998, wind stress is determined directly from NCEP operational analysis. Transients resulting from the wind forcing changes are minimized by gradually applying a new forcing over 6 months. Surface heat flux for 1980–1996 was the mean annual climatological cycle of *Oberhuber* [1998]. From 1997 onward the heat flux is taken from the NCEP operational analysis. The impact of these changes has not been quantified.

[16] The heat content is computed using data for the upper 387.5 m (using model levels down to and including 345 m but excluding levels at 430 m and below), based on the fact that most expendable bathythermographs sample this layer but not deeper and there is inadequate information at greater depths to determine interannual variability. However, it is apparent that the main variability is above 300 m depth, and contributions from deeper layers are believed to be very small. We compute the heat content H as

$$H = \sum_i \rho C_p T_i \delta z_I \qquad (3)$$

over the available layers i. In computing the heat content, given that the maximum variability in temperature is in the thermocline and we are interested primarily in the tropics and subtropics of the Pacific, we have selected constants of 1025 kg m^{-3} for density ρ and 3990 J kg^{-1} K^{-1} for C_p that correspond approximately to a temperature of 20°C, salinity of 35–35.5 per mil, and 100–150 m depth. The product ρC_p is representative of a much broader range of values, because C_p increases with temperature while density decreases.

[17] Because large natural variability on synoptic timescales appears as weather noise in monthly means and there is spurious noise related to sampling (especially for SSTs, OLR, subsurface ocean temperature, and $\nabla \cdot \mathbf{F_A}$), we have smoothed the monthly anomaly fields used in the analyses with a binomial (1, 2, 1)/4 filter, which removes 2-month fluctuations. We primarily employ correlation and regression analysis to bring out relationships at various lags.

[18] For correlations between variables with persistence related to ENSO for the 240 months from 1979 to 1998, we estimate that there are ~80 degrees of freedom, suggesting statistical significance at the 5% level if the correlations exceed ~0.23 [see *Trenberth*, 1984]. However, as the linkages are well established as real, we use the correlations to determine the patterns and regions that contribute to the global relationships.

3. Tropical Pacific Variability

3.1. Tropical Pacific and Links With Global Mean Temperature

[19] As noted in section 1, we use N3.4 as the key ENSO index. The N3.4 index given in Figure 1 is normalized using the means
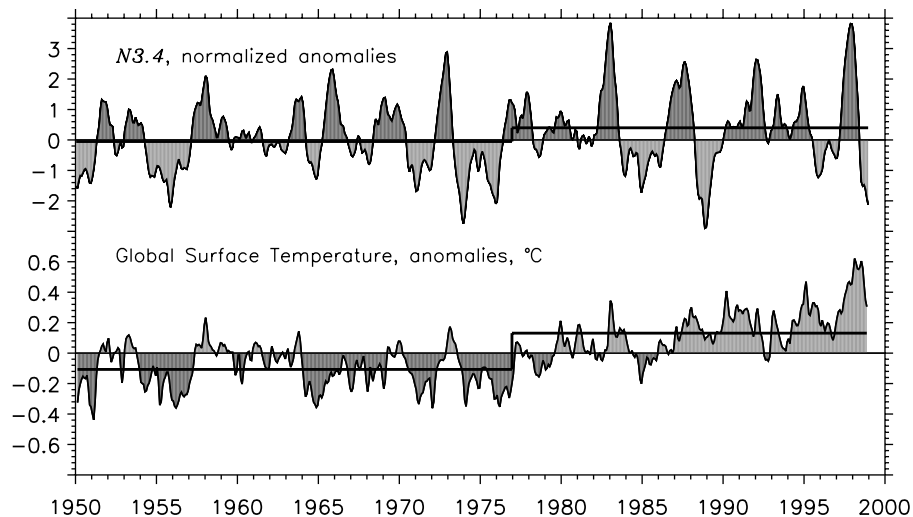
Figure 1. Time series of (top) Niño 3.4 SST (N3.4) and (bottom) the global mean temperature for 1950–1998. Base period for N3.4 is 1950–1979. Means for 1950–1976 and 1977–1998 (horizontal lines) are shown separately to highlight the climate shift in 1976/1977.

and standard deviations for 1950–1979. Cross correlations of N3.4 and the Southern Oscillation Index based upon surface pressures at Tahiti and Darwin are a maximum at zero lag (−0.83) for 1950–1998 and for the two subperiods. Also presented in Figure 1 is the global mean surface temperature along with the means before and after 1976/1977 for both series to illustrate the shift that occurred toward warmer and more El Niño-like conditions in the late twentieth century.

[20] For the global mean temperatures for 1979–1998, the cross correlations (Figure 2) reveal a broad maximum with the global

Figure 2. Cross correlations between N3.4 and global mean temperature for 1950–1978, 1979–1998, and 1950–1998 as a function of lead and lag. Positive values mean that N3.4 leads.

mean temperature lagging N3.4 by 4 months. This is less than is found in several other studies, for reasons that are not fully clear. In part, it appears to relate to different ENSO indices that are used, and some are not optimal [*Trenberth*, 1984]. *Wigley* [2000] attempts to remove the cooling effects of the two volcanic eruptions (El Chichon and Pinatubo) after which the relation between ENSO and the global mean temperature becomes stronger. The result highlights the convolution of the volcanic signal and ENSO event during this period with a blurring of the ENSO-related relationships as a consequence. It reinforces the need in Figure 2 and subsequent analysis to also explore the relationships for the 1950–1978 period. Figure 2 shows that the lag correlations are higher and more sharply peaked in the 1950–1978 period than more recently, again strongly suggesting either a contaminating influence from the two major volcanic eruptions or an impact of the 1976/1977 climate shift or both. The lag is sharply defined as 3 months, with a peak correlation of 0.65, corresponding to a regression of 0.11°C per N3.4, compared with 0.08°C for 1979–1998.

[21] The 1976/1977 climate shift, whether part of decadal variability or trend, influences results when the two subperiods are combined. Therefore it is worthwhile to include results for the entire period 1950–1998, as the different means in the two subperiods factor into the results. The correlations for the entire period are intermediate between those of the two subperiods except that positive correlations last longer (−10 to +16 months) and are centered at +3-months lag. Negative correlations before and after the positive peak, which signal the ENSO quasiperiodicity, are less in evidence on the longer timescale, reflecting the influence of the 1976/1977 climate shift. Alternatively, there is a significant linear trend to the global mean temperatures that accounts for 41% of the total variance for 1950–1998.

[22] Finally, in this subsection we examine how much variance of the global mean temperature is accounted for by ENSO for 1950–1998 using regression and the residual series (Figure 3). The maximum lag correlation between N3.4 and global temperature is 0.53 (28% of the variance) at +3 months. Surprisingly, this is identical whether or not the two series are detrended. The regression coefficient based on the detrended relationship is 0.094°C per N3.4 and is deemed more appropriate. The N3.4 contribution is given in Figure 3. It shows that for the 1997–1998 El Niño, where N3.4 peaked at ∼2.5°C, the global mean temperature was elevated as much as 0.24°C (Figure 2), although, averaged over the year centered on March 1998, the value drops to ∼0.17°C. The linear
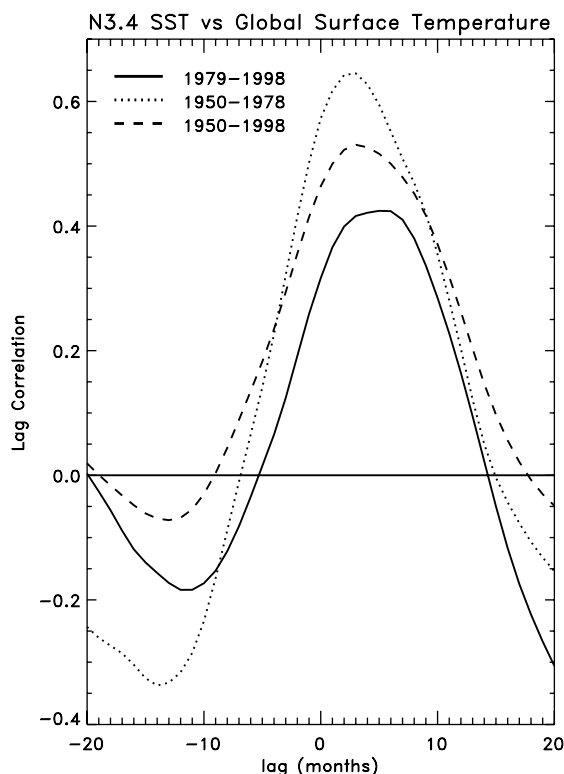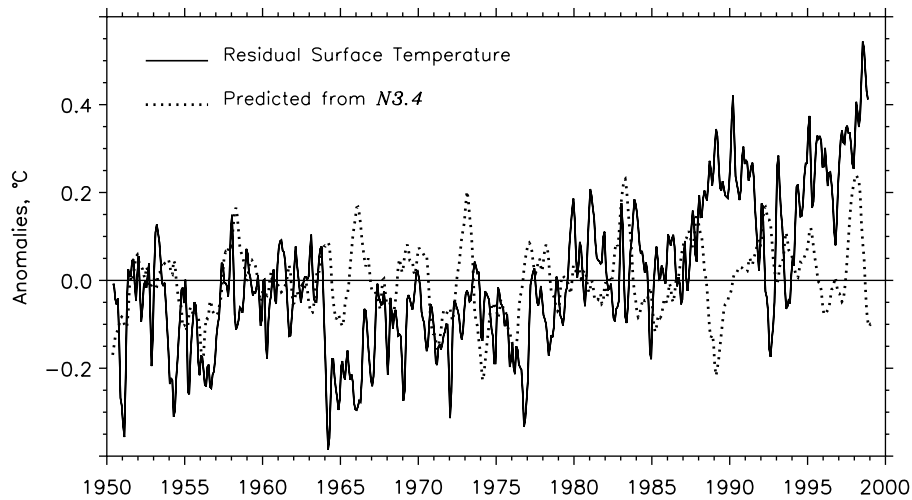
Figure 3. Global mean temperature residual anomalies (solid line) after the linear effects of El Niño–Southern Oscillation (ENSO) (dotted line) are removed using the N3.4 index.

Zonal Mean Lag Correlations with Niño 3.4 SSTA
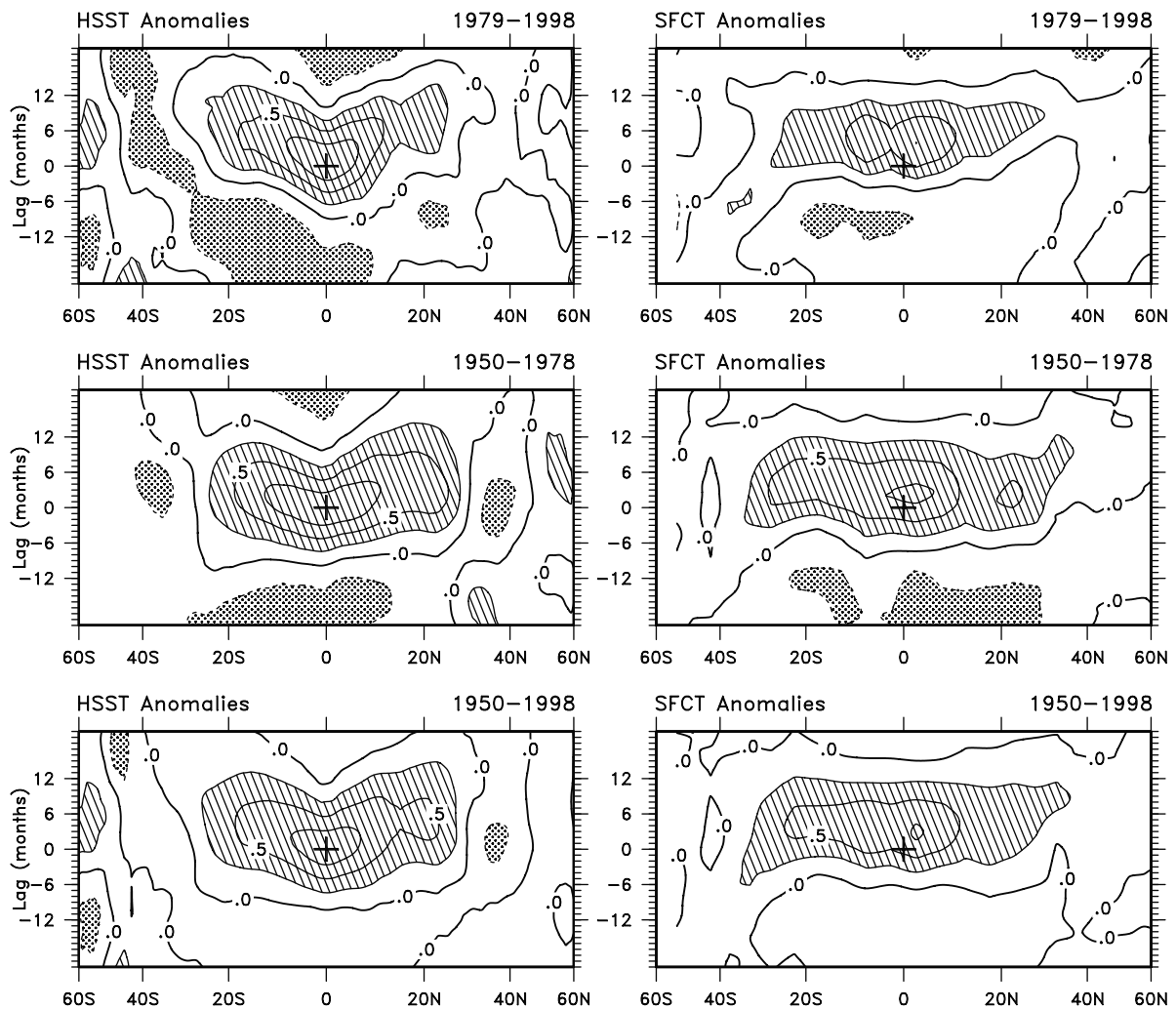
Figure 4. Cross correlations of N3.4 with zonal means as a function of latitude of (left) sea surface temperature (SST) and (right) surface land temperature for (top) 1979–1998, (middle) 1950–1978, and (bottom) 1950–1998. Positive values mean that N3.4 leads. Values exceeding 0.25 are hatched, and values less than −0.25 are stippled.
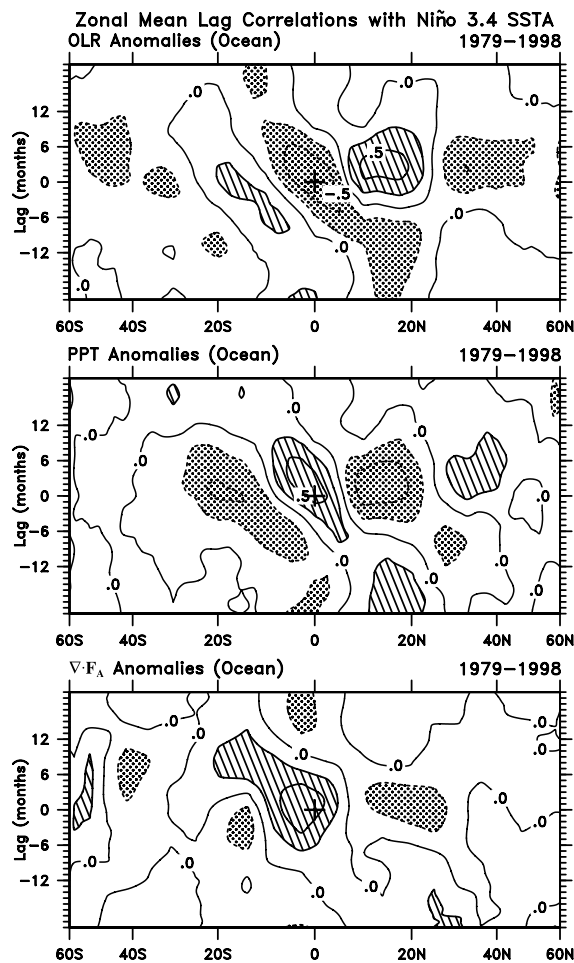
Figure 5. Cross correlations of N3.4 with zonal means over the ocean of outgoing longwave radiation (OLR), precipitation, and $\nabla \cdot \mathbf{F_A}$. Values are shown as in Figure 4.

trend in N3.4 over 1950–1998 accounts for 4.1% of the N3.4 variance and further accounts for 1.8% of the variance due to the trend in global mean temperature. As this is based on the regressions using detrended data, the relationship is determined by the interannual variations. It means that 13.6% (=$0.018^{0.5}$) of the linear trend in surface temperature, or 0.06°C for 1950–1998, arises from the changes in ENSO (out of 0.43°C).

3.2. Zonal Mean Results

[23] Figure 4 presents cross correlations of N3.4 with zonal means at leads and lags as a function of latitude. Positive values always refer to N3.4 leading. Figure 4 shows results for (top panel) 1979–1998, (middle panel) 1950–1978, and (bottom panel) the full period 1950–1998. For SSTs (Figure 4, left-hand column) the maximum correlations exceed 0.8 from 2 months before to 3.5 months after N3.4 and reversing in sign a year before and a year after for 1979–1998. Correlations outside about ±30° are not significant. However, of considerable interest are the "wings" or lobes of positive correlations extending from the equatorial region into the subtropics a year later. For 1950–1978 the leads and lags in the equatorial region are more symmetric although the wings into the subtropics are still present, and this pattern also exists for the entire period, without diminution of the correlations, and thus there is an enhancement in statistical significance.

[24] The equivalent results for the full surface temperatures (not shown), which thus include land portions, are quite similar overall, although the central highest correlations are delayed by 2 months

in the equatorial region and positive values are slightly higher in the subtropics a year later. As with SST, there is no evidence of any relationship extending to higher latitudes, although such has been claimed by *Angell* [2000]. Therefore Figure 4 (right-hand column) shows the results just for land. Over land, there is less evidence for delays with increasing latitude, but the whole pattern is delayed by 3–4 months. The extension is to slightly higher latitudes, especially in the Northern Hemisphere where correlations from 45°N–50°N exceed 0.2 at 0- to 7-months lag, and correlations are 0.2 at 65°N at 13-months lag. This is more consistent with Angell's result and indicates that it is probably biased by the distribution of stations used by Angell.

[25] Shown in Figure 5 are lag correlations for 1979–1998 of OLR, precipitation, and $\nabla \cdot \mathbf{F_A}$ with N3.4 for the ocean only. Because the main precipitation algorithm over the oceans uses OLR (low OLR from high cloud tops corresponds to high convective rainfall), the OLR and precipitation results are very similar. We have examined the corresponding correlations for just the Pacific Ocean and also for the globe (including land). For $\nabla \cdot \mathbf{F_A}$ the land values are unreliable and are not useful [*Trenberth et al.*, 2001]. The main relationship over the oceans comes from the Pacific, where the correlations exceed 0.8 just south of the equator near lag 0, but with a pattern quite similar to that shown in Figure 4. For precipitation the patterns for the Pacific versus total ocean versus global zonal means (not shown) are quite similar, although positive correlations decrease in the near-equatorial region and
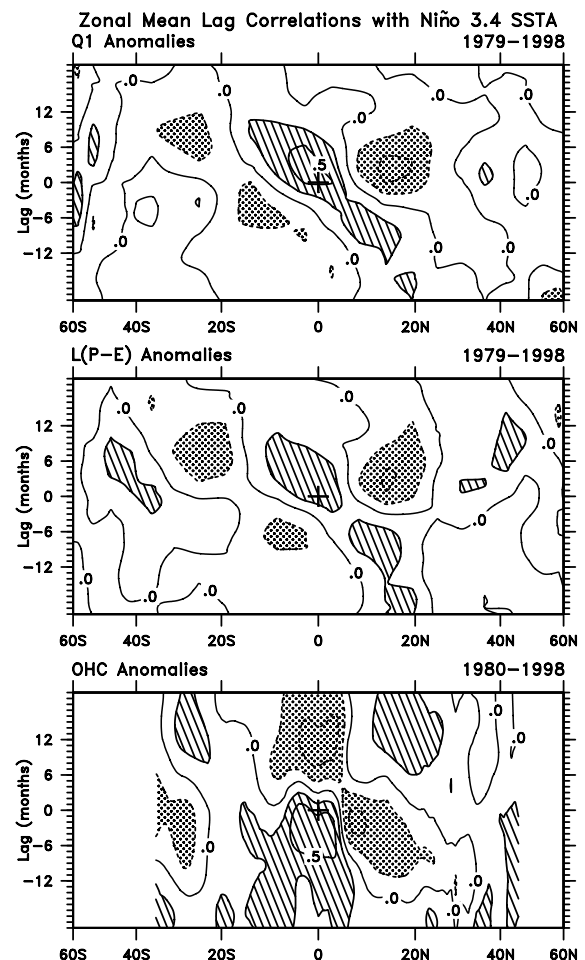
Figure 6. Cross correlations of N3.4 with zonal means over the ocean of Q_1, $L(P - E)$, and Pacific Ocean heat content. Values are shown as in Figure 4.

N3.4 SST vs. Surface Temperature
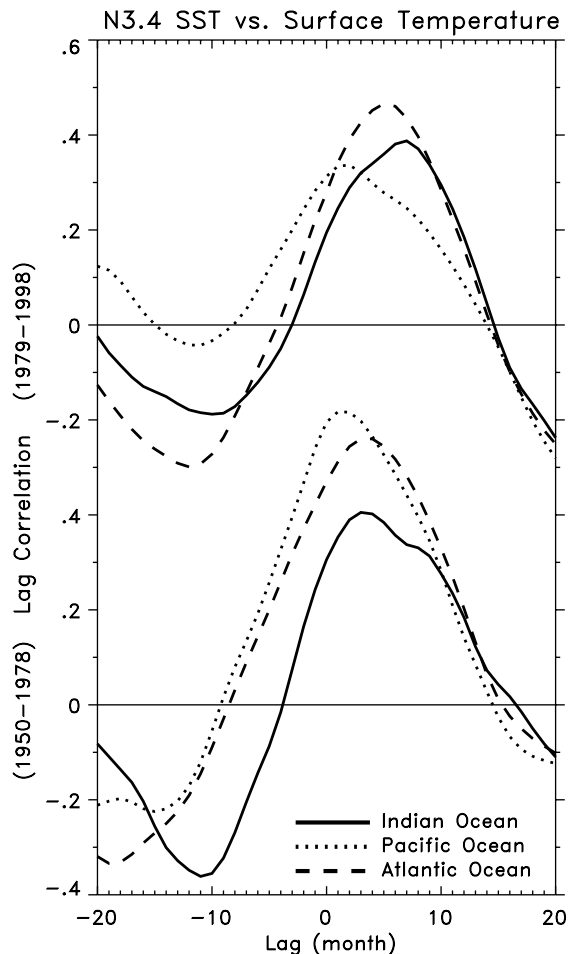
Figure 7. Cross correlations between N3.4 and mean surface temperature over three sectors, Pacific (120°E–90°W), Atlantic (90°W–0°), and Indian (0°–120°E), for (top) 1979–1998 and (bottom) 1950–1978 as a function of lead and lag. Positive values mean that N3.4 leads.

negative correlations in the subtropics hold steady in all three domains. For both precipitation and $\nabla \cdot \mathbf{F_A}$ the lagged relationship indicated by the wing into the Northern Hemisphere is absent and only the wing in the Southern Hemisphere is present. As seen in section 3.3, this wing arises from the changes in the South Pacific Convergence Zone (SPCZ).

[26] Figure 6 shows ocean-only zonal means for several other quantities: the vertically integrated atmospheric diabatic heating $(Q_1 - Q_f)$, $L(P - E)$ from the moisture budget [*Trenberth et al.*, 2001], and the ocean heat content in the Pacific. The patterns are almost identical for the land plus oceans combined. The $L(P - E)$ relationship is similar to but much weaker than that for precipitation alone. The diabatic heating, computed from the thermodynamic equation as a residual, is quite similar to that for precipitation, as would be expected if latent heating is dominant, although the fact that it is slightly weaker is probably a deficiency in the NCEP reanalyses [*Trenberth and Guillemot*, 1998].

[27] The correlations with upper ocean heat content in the Pacific, on the other hand, are quite different in character. Figure 6 reveals strong correlations, indicating the buildup in equatorial heat from 12 to 6 months prior to the peak in N3.4, with the maximum correlation occurring 4 months prior to N3.4. Meanwhile, there is cooling from 5°N to 20°N that is a maximum at 8°N 2 months before N3.4. Significant cooling also follows the peak in

the equatorial region culminating ∼12 months after N3.4, but the off-equatorial correlations are not as strong, suggesting some loss of signal through diabatic effects. This pattern is consistent with that depicted by *Meinen and McPhaden* [2000].

3.3. Evolution of Spatial Patterns

[28] Figure 7 shows a breakdown of Figure 3 by ocean sector for 1950–1978 and 1979–1998. It seems obvious that the lag of surface temperatures in the Pacific should be closely in phase with N3.4 because of the close proximity, and indeed this is the case, with a 2-month lag in both subperiods. However, the peak correlation is almost doubled in the earlier period. The Atlantic sector (defined as 90°W–0°) lags by 4–5 months, while the Indian Ocean sector (defined as 0°–120°E) shows a lag of 7 months for 1979–1998 but a skewed and smaller lag centered around +5 months from 1950 to 1978. The corresponding regressions have peak values of 0.10°C in the Indian and Atlantic sectors versus 0.06°C for the Pacific for 1979–1998 and 0.12°–0.13°C for all three oceans for 1950–1979. These results highlight the need to examine the redistribution of heat spatially.

[29] To explore where the heat in the oceans and its effects on the atmosphere actually occur, we have computed correlation and regression maps for several fields at various lags, a subset of which are given here. Generally, the regression maps are quite similar in overall patterns, but the correlations are presented as they allow significance to be roughly assessed. Figure 8 presents a sequence of lagged correlations of N3.4 with surface temperatures (based on the NCEP SSTs over the ocean blended with the UEA land data) for 1979–1998 (Figure 8, right-hand column) at −8, −4, 0, 4, and 8 months. Once again, positive values signify that N3.4 leads. This sequence reveals the mean evolution of ENSO and is quite coherent and traceable from about −12- to +12-months lag with N3.4, but becomes quite weak at larger lags. The panels presented in Figure 8 and the Δ4-month sequence are chosen to illustrate the evolution in the fewest panels. Figure 8 (left-hand column) presents the same sequence for surface temperatures from 1950 to 1978.

[30] For 1979–1998 the maximum warming in the central equatorial Pacific following El Niño develops from off-equatorial tropical regions and from the west, progressing eastward. In contrast, for 1950–1978 the anomalous warming begins strongly along the coast of South America and appears to spread westward, as was found by *Rasmusson and Carpenter* [1982]. This difference in development continues. The eastern Pacific south of the equator from +4 to +8 months warms during 1979–1998 but cools during the 1950–1978 period. In the Indian Ocean, warming begins 4 months prior to the peak in N3.4 and is strongest from 0 to +4 months for 1950–1978 and at +4 months for 1979–1998 and is still strongly evident at +8 months. The Atlantic signal becomes strongest at about +4 months and is quite similar in the two periods, with warming mainly from 0° to 25°N but also some warming at ∼20°S. These results are consistent with those of *Klein et al.* [1999] for the tropical Atlantic and Indian Oceans.

[31] Figure 9 (left-hand column) presents the same sequence except as lag regressions for the entire period (1950–1998). It therefore highlights the land surface temperature signal that is the same between the two subperiods and converts the signal into actual temperature anomalies, thereby sharpening the focus on the tropical Pacific and extratropical North America, where the variance is greater than over the rest of the oceans. Referring to the ENSO warm phase, at lag 0 the warmth in the tropical central and eastern Pacific is accompanied by substantial warmth along the west coast of the Americas, especially in the western two thirds of Canada and Alaska, and is mirrored to some extent in the South Pacific near 50°S–60°S. Modest but widespread warmth is also evident in the Indian Ocean, Africa and southern Asia, and in bands from South America across the Atlantic near 20°N and 30°S. The effects in the Atlantic and Indian Ocean sectors become strongest at about +4 months and are still evident at +8 months.
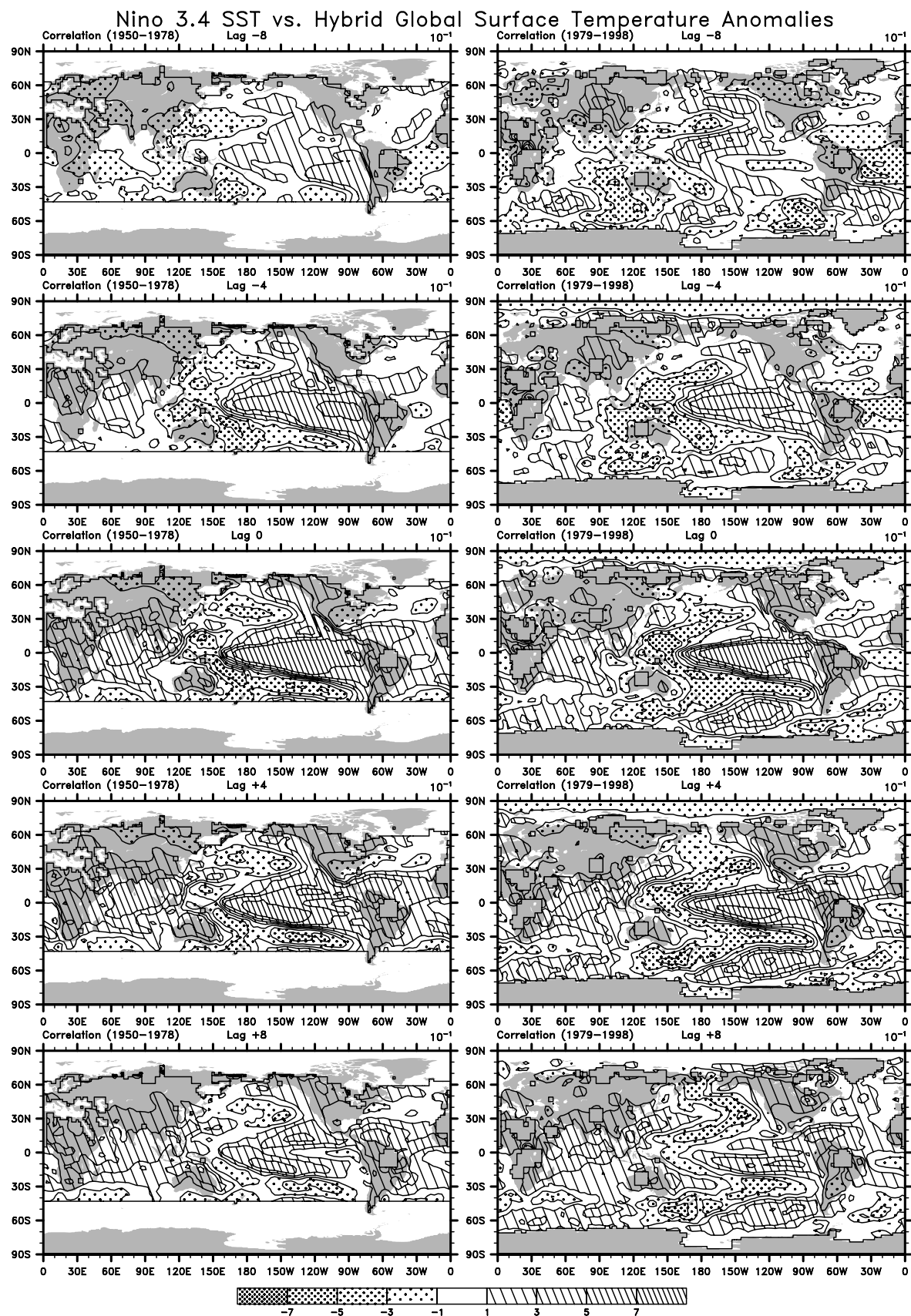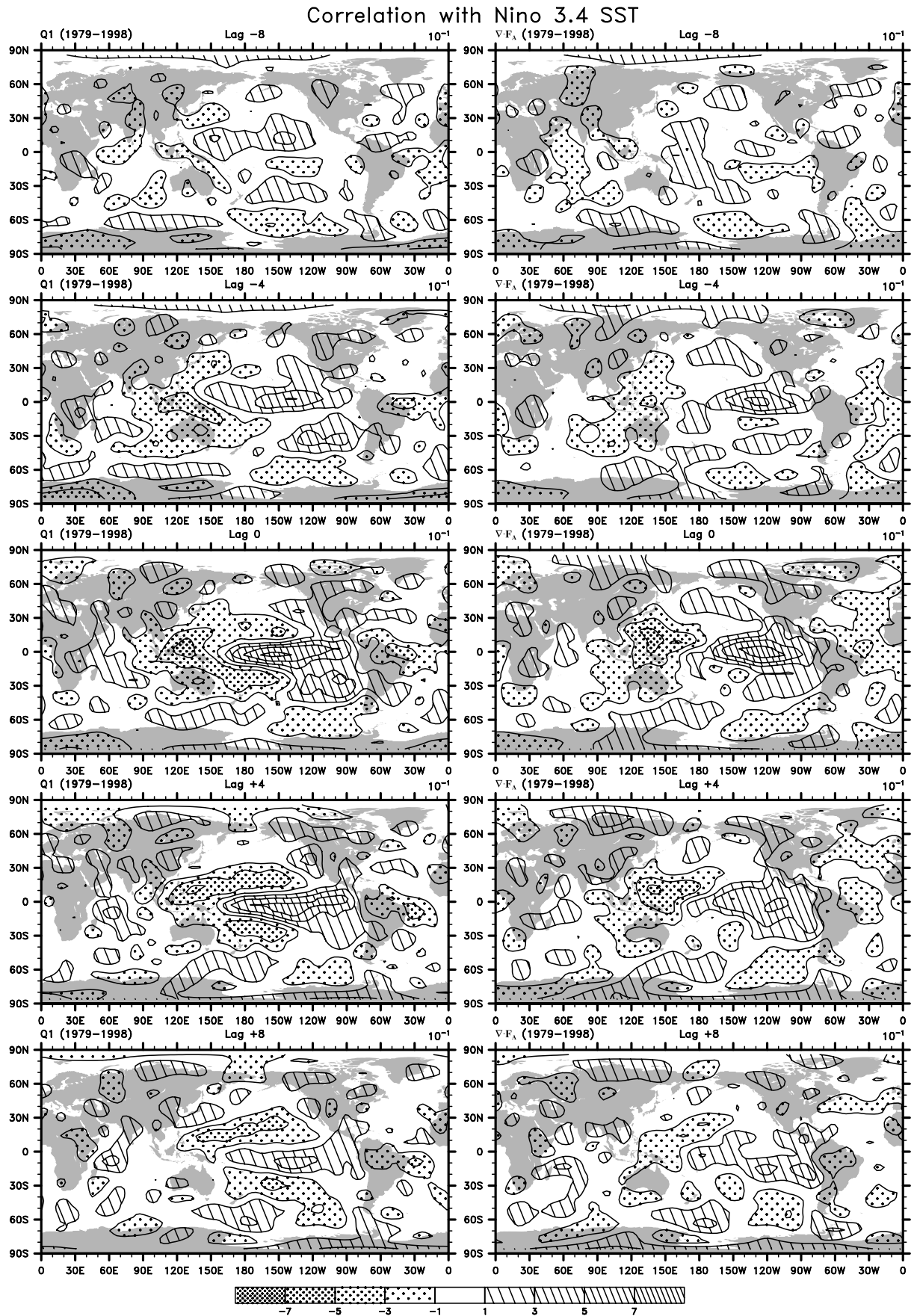
Figure 8.   Time sequence of correlations (×10) with N3.4 of surface temperatures (based on the Reynolds SSTs over the ocean blended with the University of East Anglia land data) for (left column) 1950–1978 and (right column) 1979–1998 at −8, −4, 0, 4, and 8 months. Color contour interval is 0.2. See color version of this figure at back of this issue.
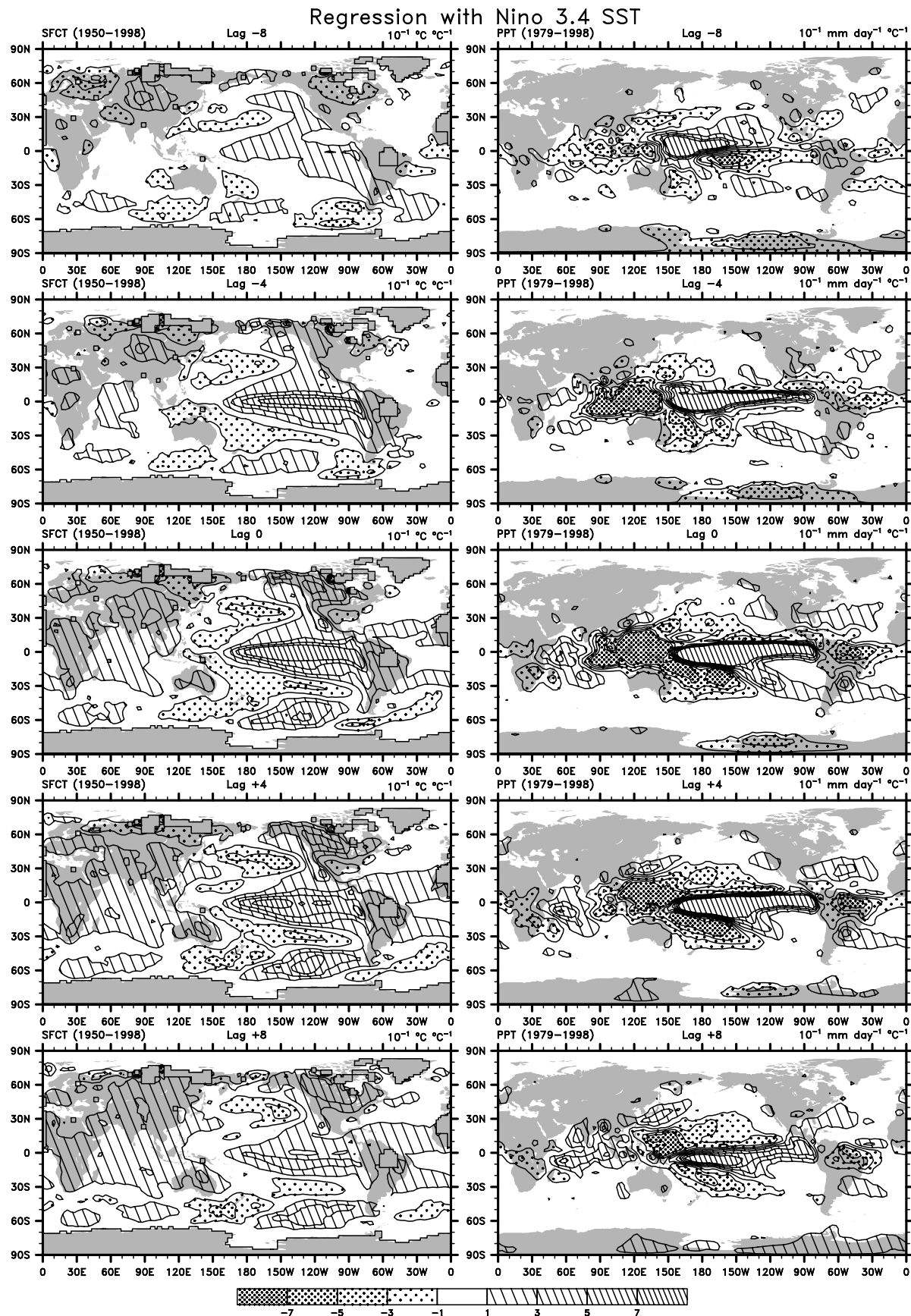
Regression with Nino 3.4 SST

Figure 9. (left) Time sequence of regression coefficients with N3.4, as in Figure 8, but for surface temperatures for 1950–1998 in tenths degrees Celsius and (right) precipitation for 1979–1998 in millimeters per day per N3.4 in degrees Celsius. See color version of this figure at back of this issue.

Figure 10. Time sequence of correlations with N3.4, as in Figure 7, but for (left) vertically integrated atmospheric diabatic heating and (right) $\nabla \cdot \mathbf{F_A}$ for 1979–1998. See color version of this figure at back of this issue.
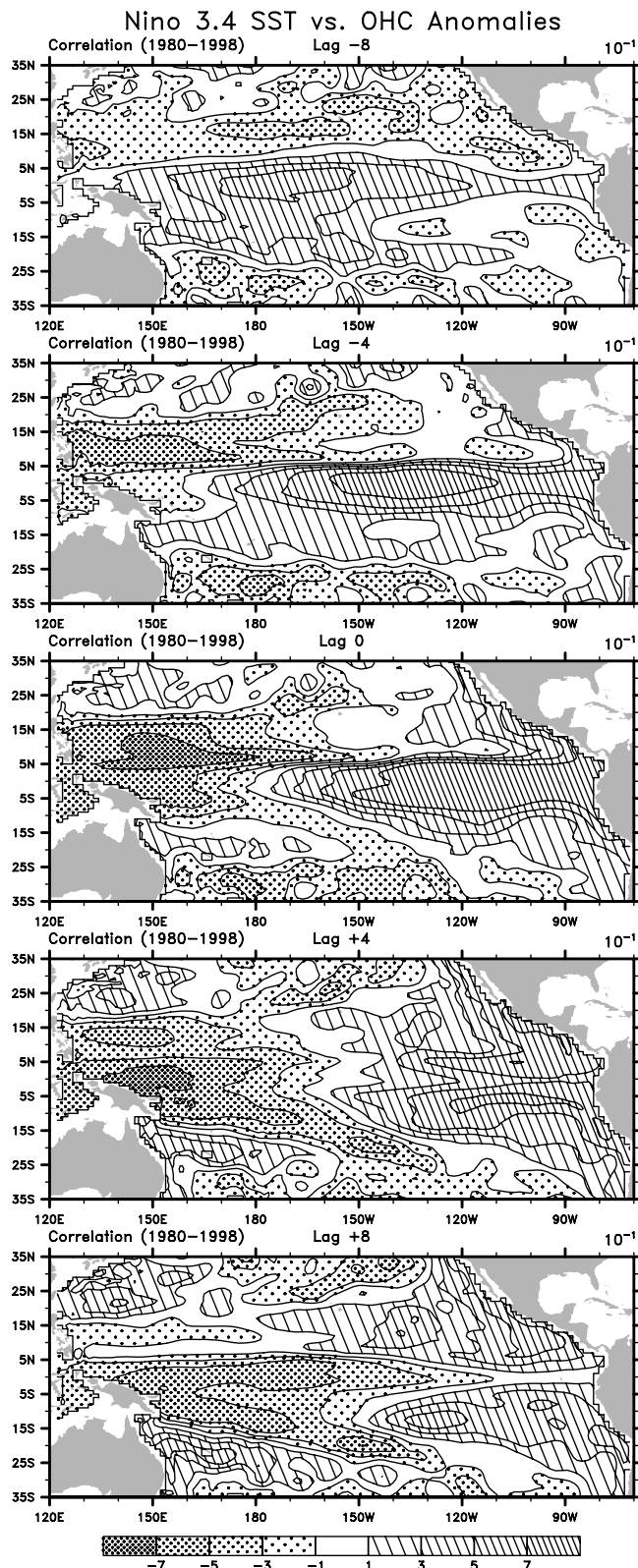
Nino 3.4 SST vs. OHC Anomalies

Figure 11. Time sequence of correlations with N3.4, as in Figure 7, but for Pacific Ocean heat content for 1980–1998. See color version of this figure at back of this issue.

et al., 1999]. Similarly, drier conditions over Southeast Asia (mainly prior to 1977 [*Kumar et al.*, 1999]; see also the differences in Figure 8) and parts of Africa imply warmer temperatures in the summer half year, as shown next.

[32] Figure 9 (right-hand column) therefore also presents the regression sequence of N3.4 with precipitation, but only for 1979–1998. The pattern is, not surprisingly, almost identical with OLR

N3.4 SST vs. Ocean Heat Content
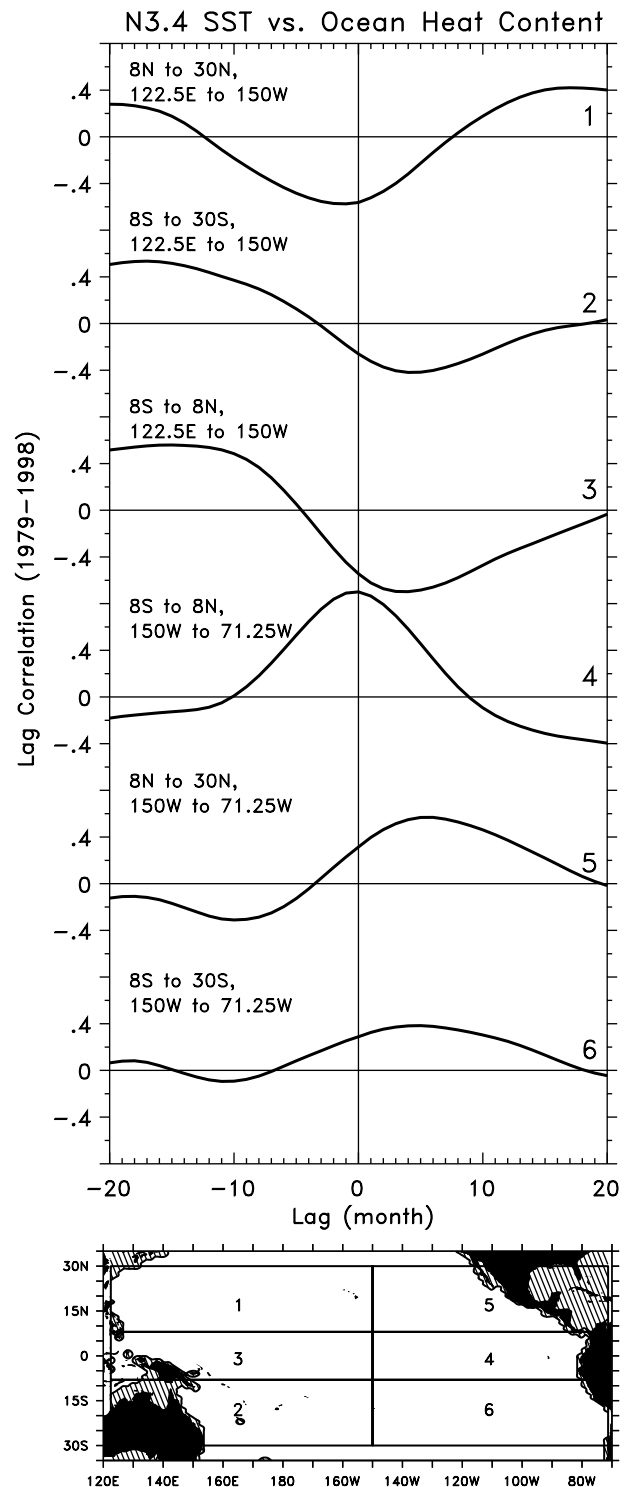
Figure 12. Time sequence of lag correlation with N3.4 from −20 to +20 months of the ocean heat content in six domains, numbered 1 to 6, as shown.
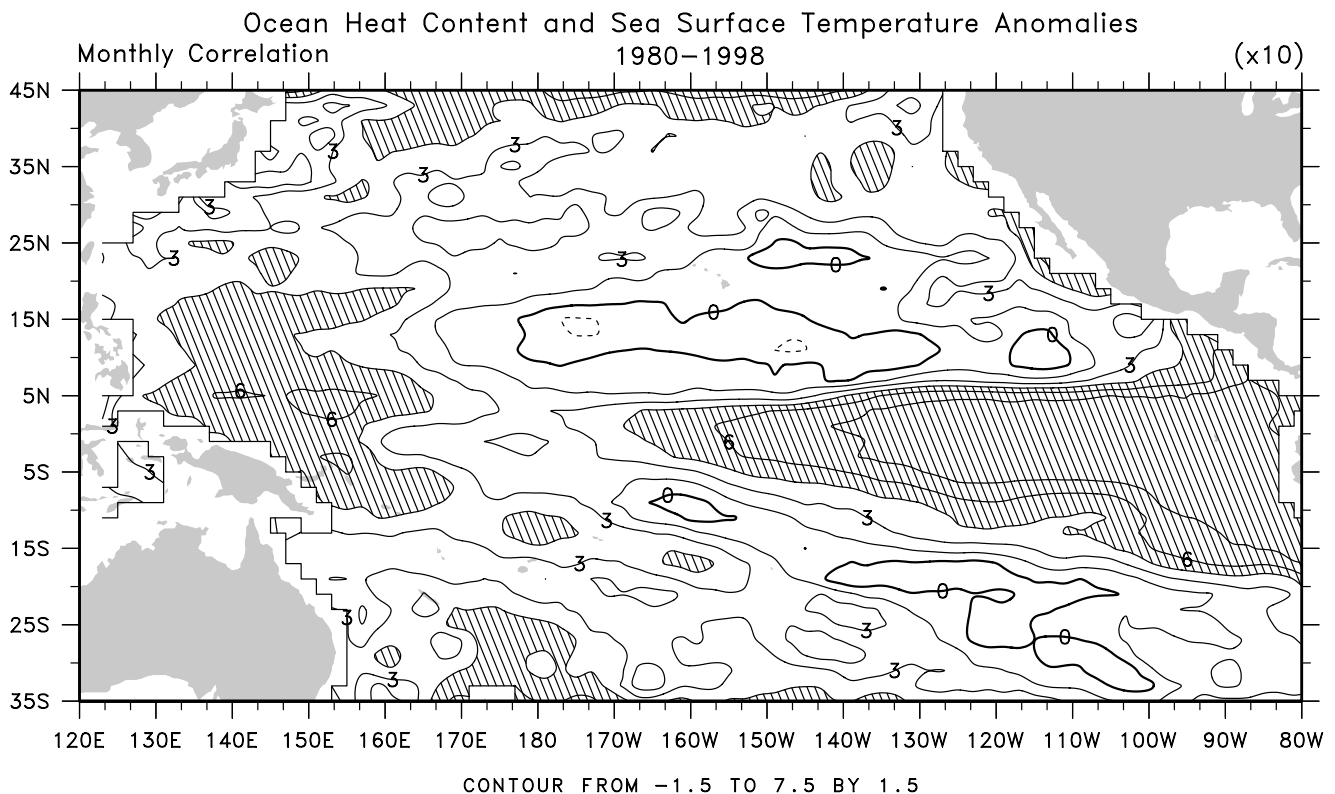
Australia also tends to be warm from 0 to +8 months. The latter relates to the relatively dry, or even drought, conditions during El Niño and so is at least partly a result of changes in cloudiness and atmospheric circulation and not just of heat from the ocean [*Klein*

Figure 13. Correlation between monthly anomalies in local heat content and SST over the period 1980–1998. Values >0.45 are hatched.

(not shown), except that the units are different. Peak values of order 1 mm day^{-1} per standard deviation of N3.4 in precipitation correspond to ∼10 W m^{-2} in OLR and correlations over 0.5 in magnitude. The strong east-west dipole and boomerang pattern in ENSO is familiar and has very large cancellation when zonally averaged, as in section 3.2. Because much of these patterns arises from northeastward movements of the SPCZ and southward movements of the Intertropical Convergence Zone (ITCZ), the dividing lines are sharp and do not match the SST changes, although there is a general tendency for wetter and warmer conditions to coexist in the tropical oceans. Over land the relationship is rather different, and warmer conditions more often than not go hand-in-hand with drier conditions, symptomatic of the changes in monsoons that occur with ENSO.

[33] The relationships with the inferred vertically integrated diabatic heating of the atmosphere and $\nabla \cdot \mathbf{F_A}$ (Figure 10) are similar to those at zero lag given by *Trenberth et al.* [2002]. The diabatic heating pattern tends to be similar to that of precipitation, signifying the dominance of the latent heating anomalies. It is also closely related to anomalies in mean vertical motion in the midtroposphere (not shown). The positive correlations between $\nabla \cdot \mathbf{F_A}$ and SST anomalies in the Pacific are reversed in middle and higher latitudes and in the tropical Atlantic. Although a clear sequence of $\nabla \cdot \mathbf{F_A}$ anomalies can be discerned in Figure 10, it is not as strong as with some other fields, and the pattern is strongest at 0 and +4 months, suggesting that it is mainly a response to ENSO.

[34] The evolution of the Pacific Ocean heat content anomalies (Figure 11) shows patterns that have been partly documented elsewhere, as noted in section 1. The buildup of heat in the western Pacific occurs before −8 months, progresses eastward to reach the west coast of the Americas before lag 0, and subsequently spreads poleward into both hemispheres (+4) and then westward from 10°N to 20°N at +8 months. There is a buildup near 10°S but with little spread westward beyond ∼150°W, near the location of the

SPCZ. Figure 12 extends the time sequence by focusing on what appear to be fairly coherent regional averages. This shows that the buildup of heat in the western Pacific, west of 150°W, first occurs off the equator (−20 to −18 months), most strongly south of 8°S. It progresses into the equatorial region (8°N−8°S), peaking at about −15 months. The equatorial and southern regions west of 150°W become negative at −3 and −5 months, and the maximum negative correlation is at +4 or +5 months. Meanwhile, the initial heat deficit from 8°N to 30°N, which peaks at −5 months, becomes positive at +4 months and peaks at +14 months. The maximum heat content from 150°W to the Americas in the ±8° latitude strip coincides with N3.4 and drops to zero at +9 months. From 8°S to 30°S, east of 150°W, the warming occurs from −7 to +18 months, peaking at +5 months.

[35] While the changes in Pacific heat content lead and appear to determine the SST evolution in the equatorial strip, this does not seem to be the case at higher latitudes. This is shown by the local correlation between the monthly anomalies of ocean heat content and SST (Figure 13), which has direct implications for the ability of a simple two-layer ocean model to depict SST variations corresponding to variations in the local thermocline. Only in the equatorial region, broadening from 20°N to 10°S west of 170°E and from 10°N to 15°S along the Americas, is the correlation significantly positive. Values are actually negative along most of the Pacific at 10°N−15°N, north of the ITCZ, and also just northeast of the SPCZ region from 10°S 160°W to 35°S 100°W. *Giese and Carton* [1999] show a somewhat similar figure based on model assimilated data. This result directly reflects the ability of the subsurface ocean heat to have a sustained influence on the atmosphere.

4.   Discussion

4.1.   Role of the Tropical Pacific Ocean

[36] In the tropical Pacific, and in the tropical Indian Ocean to some extent [*Tourre and White*, 1995], heat loss from the ocean

drives the atmospheric circulation changes. The redistribution of heat by ocean currents as ENSO evolves contributes directly to subsequent heating and increased temperatures in the tropics and subtropics as El Niño fades. Magnitudes of observed changes in surface fluxes with moderate El Niños are ~40 W m^{-2} [*Trenberth et al.*, 2001], which corresponds to a 1°C temperature change over a column of water of 130 m deep over 5 months. Zonal means across the Pacific of the ocean heat content (not shown) reveal typical anomalies of order 0.5×10^9 J m^{-2} over 5° latitude, which corresponds to a 1°C change over a layer of 122 m. Maximum zonal mean anomalies in 1981–1983 and 1997–1998 are ~3 times this value, but these are the main occurrences that feature a meridional dipole with anomalies of opposite sign, signifying a rearrangement of heat within the ocean. Consequently, the estimated surface heat fluxes are a dominant factor in the change in area-average subsurface ocean heat content, and the heat is transmitted to the atmosphere.

[37] The evolution of ENSO in the tropical Pacific Ocean illustrated here supports much of that previously described by *Barnett et al.* [1991], *Zhang and Levitus* [1996], *Tourre and White* [1995], *Giese and Carton* [1999], *Smith* [2000], and *Meinen and McPhaden* [2000] in the way that anomalies of subsurface ocean heat content in the western Pacific develop as they progress eastward across the equatorial Pacific, often with a dipole pattern across the Pacific, and then with anomalies progressing off the equator to higher latitudes. *Zhang and Levitus* [1996] found links only to the North Pacific, perhaps reflecting the available data, while our results reveal strong links to both hemispheres. The SST evolution lags somewhat behind that of the subsurface ocean and is damped by surface fluxes and transports out of the region by the atmosphere, emphasizing the dominant role of the surface wind stress and ocean dynamics and advection in producing the local ocean heat content and SST anomalies. This damping of the ocean signal, however, forces the atmospheric anomalies. Moreover, this aspect also emphasizes that in cold La Niña conditions the surface fluxes of heat are going into the ocean relative to the mean and are warming the ocean, although not locally as the heat is redistributed by currents.

[38] The evolution of the ocean heat content shows the eastward progression in the equatorial region, then the spreading north and southward (presumably as Kelvin edge waves) along the west coast of the Americas to higher latitudes, but also with a component spreading westward at ~10°–20° latitude in both hemispheres. From 1979 to 1998 the SSTs were strongly positive in the Southern Hemisphere but remained negative in the Northern Hemisphere 12 months after the N3.4 index peaks. The SST development from 1950 to 1978 is rather different and results in strong positive anomalies in the Northern Hemisphere near 10°N–20°N 12 months after the peak, with some residual heat in the Southern Hemisphere in a region where it can influence the SPCZ. As previously emphasized, there has been quite different evolution along the coast of South America in the classical El Niño region. Warming at the surface tended to occur first along the coast of South America before 1979, as in the *Rasmusson and Carpenter* [1982] composites, but in more recent years the coastal warming followed that in the central Pacific [*Wang*, 1995].

4.2. Role of the Atmosphere

[39] In dealing with a time mean atmospheric heat budget over several months, tendencies are necessarily small, and all the terms must be in balance. As a result, the cause of a temperature anomaly may not be easily deduced, and the utility of quantities like $\nabla \cdot \mathbf{F_A}$ is limited.

[40] There is little to support the idea that the local ocean heat storage plays much of a role at higher latitudes. Instead, there is a known strong link through atmospheric teleconnections between ENSO events and changes elsewhere [*Trenberth et al.*, 1998]. Over the North Pacific, ENSO teleconnections are well captured at the

surface by the index of area-average sea level pressure over the North Pacific, called the NP index [*Trenberth and Hurrell*, 1994]. Cross correlations between N3.4 and NP (not shown) are negative for −5- to +10-months lag and peak at −0.20 at +2-months lag for 1979–1998. That relationship is strongest in the winter half year. Composites of seasonal anomalies of mean temperature, changes in storm tracks, and tendencies in temperature from divergence of transient eddy heat transport [*Trenberth and Hurrell*, 1994] show that the latter two are negatively spatially correlated and act to destroy the temperature structures in the lower troposphere. Instead, the temperature perturbations are partly set up by advection by the anomalous mean flow, and this is demonstrated by regressing the 700-mbar temperature and vector wind on N3.4 as a function of lag, with N3.4 leading by 0, 4, and 8 months (Figure 14).

[41] Thus the substantial warming with El Niño over Alaska and western Canada is clearly related to the change in atmospheric circulation that is known to be forced through teleconnections from the tropical Pacific [*Kumar et al.*, 2001]. The change that most obviously brings about some warming is warm advection, and this comes about through an anomalous southerly component to the flow advecting the mean temperature gradient. We split the temperature T into the time mean, given by an overbar, and the anomaly perturbation, given by a prime, $T = \overline{T} + T'$, and split other quantities similarly. Thus it is the term $v' \, \partial\overline{T}/\partial y$ that gives rise to part of the T' (see Figure 14), while the perturbation is offset by changes in storm tracks and by the transient eddy temperature transport that acts to destroy the temperature anomaly on about a 2-week timescale [*Trenberth and Hurrell*, 1994]. These counterbalancing effects are both included within $\nabla \cdot \mathbf{F_A}$ and largely cancel. However, there is more to T' than advection, as associated changes in moisture advection and cloudiness occur, introducing some radiative anomalies.

[42] The North American warming at 700 mbar extends eastward from the maximum southerly flow to the upstream anticyclonic flow [see also *Wallace et al.*, 1998]. Over the North Pacific, Figure 14 shows the link from the cooling to the more northerly flow and also to the cyclonic circulation. An approximate mirror image appears over the South Pacific, although the wave train has a slightly shorter wavelength. Cooler conditions east of New Zealand are associated with southwesterly flow anomalies around a cyclonic circulation centered near 40°S 150°W, and a blocking high exists farther downstream near 60°S 110°W.

[43] The more complete picture, therefore, is that there is a substantial equivalent barotropic component to the atmospheric anomalies. In other words, there is a substantial temperature anomaly in phase with the geopotential height field, so that surface geopotential height or pressure anomalies increase in magnitude with height, although with some westward slope caused by the baroclinic advective component. Within the atmosphere this comes about through the potential vorticity dynamics of teleconnections [*Trenberth et al.*, 1998] in which upper tropospheric transports of vorticity and momentum by transient eddies are important along with the heat transports. To keep the system in geostrophic and hydrostatic balance, subsidence occurs in anticyclonic regions, producing warming, while rising motion in cyclonic regions results in cooling. At the surface, cyclonic flow is accompanied by Ekman transports that produce upwelling and a shoaling thermocline and by increased storminess that encourages increased ocean mixing and fluxes of heat from the ocean into the atmosphere [e.g., see *Deser et al.*, 1996]. Thus the SST signature is similar to the tropospheric signature.

[44] The remarkable persistence of the surface and 700-mbar temperature anomalies extending from at least 0 through +8 months, and thus transitioning from winter to summer seasons, is worth noting. Figure 9 shows that the tropical precipitation anomalies and thus the anomalous diabatic heating and forcing of the atmosphere in the tropics continue throughout this period.
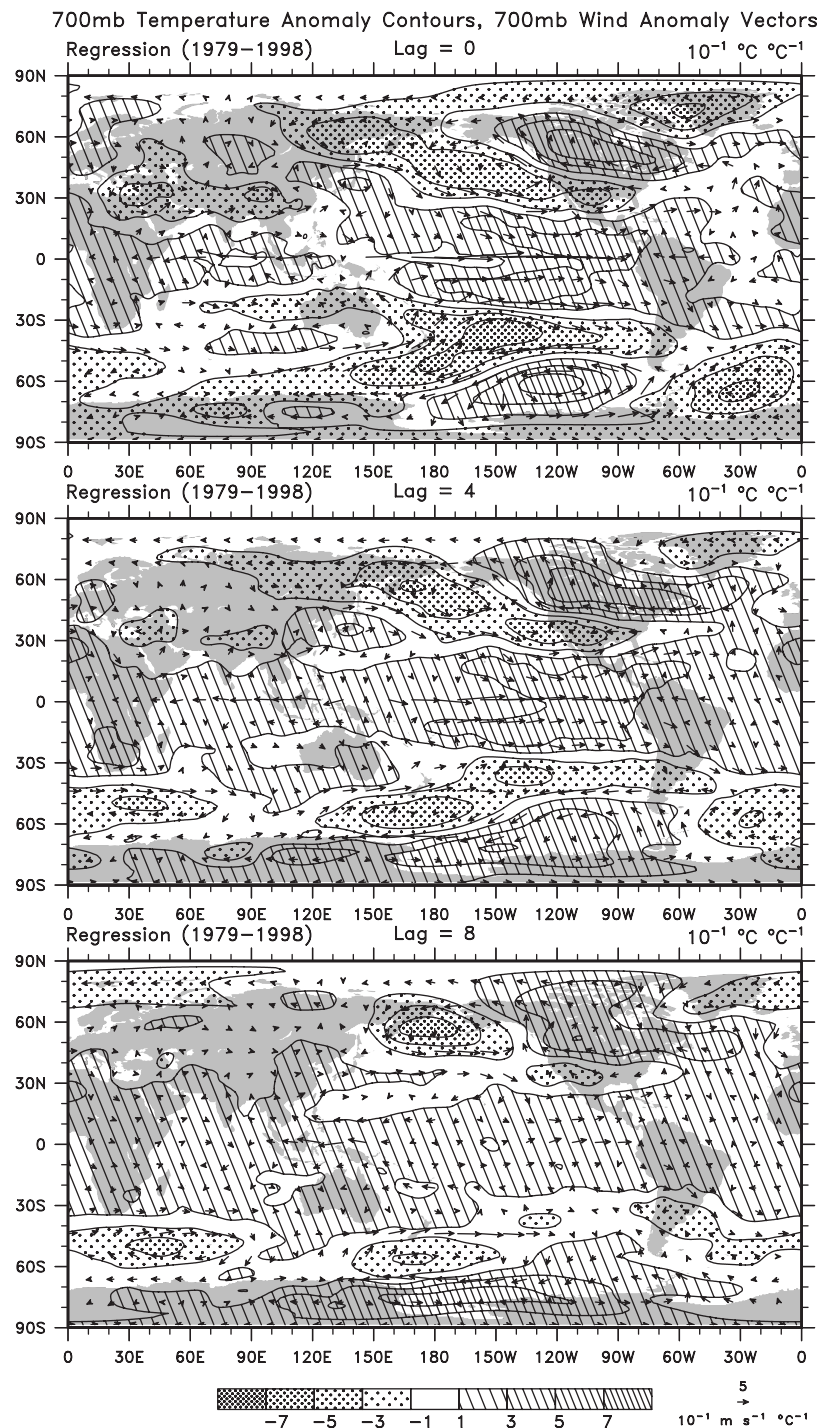
Figure 14. Regression of N3.4 with temperature and vector wind at 700 mbar at 0, 4, and 8 months for 1979–1998. For temperature the units are tenths degrees Celsius per N3.4, and the scale vector wind is given at bottom right. See color version of this figure at back of this issue.

There is some change in the anomalies with season, and at +8 months the main contrast is from the Aleutian Islands region to North America, north of 50°N (Figure 14). It is also of interest to compare the tropical precipitation (Figure 9) and diabatic heating (Figure 10) and the atmospheric response in Figures 8 and 9 for −4 and +8 months, which are for the same season but a year apart. The differences in tropical regions are fairly subtle but evidently important. At −4 months the tropical Pacific anomalies are oriented more east-west while at +8 months they involve the SPCZ, and the subtropical high near Hawaii is more involved in the tropical overturning. The response over North America is much greater in the latter case.

[45]   Hence the T' at 700 mbar is quite similar to that in Figure 8 at the surface in the extratropics, except that the cooling with El Niño over southern California at 700 mbar is not present at the surface. The latter relates to the changes in storm tracks, cloudiness, and precipitation and perhaps to some direct influence of the local warming of the subsurface ocean (Figure 11).

[46] Some nonlinear effects that come into play depend on whether the temperature anomalies occur over the ocean or land. Over the ocean the magnitude of the surface temperature change is muted by the heat capacity of the underlying ocean, the mixing of heat through the mixed layer, and possible entrainment and deepening of the thermocline. Consequently, the net surface warming over land is typically much larger than an equivalent response over the ocean (Figure 9), and this can influence the global mean temperature, although it is not equivalent to a net heat content anomaly. The changes in the North Pacific and North America are mirrored to some extent over the southeast South Pacific as anomalous blocking takes place in that region as part of the Pacific-South American teleconnection, but the land-ocean rectification effect is not present.

[47] In the tropics and subtropics over land, the predominant change is one of warming over continental land (Africa, northern South America, Australia, and southern Asia), which is associated with less precipitation, less high cloud (OLR), and more solar radiation [*Halpert and Ropelewski*, 1992; *Klein et al.*, 1999]. The dominant precipitation center moves over the central tropical Pacific, with a southward shift in the ITCZ and a northeastward shift in the SPCZ. The result is overturning teleconnections in the atmosphere that create the drier or even drought conditions in these locations. *Dai et al.* [1999] used detailed measurements from the First International Satellite Land Surface Climatology Project Field Experiment (FIFE) to document the processes involved. They show how increased precipitation and surface moisture result in more evaporation and cooler surface temperatures, whereas decreased cloud increases temperatures mainly through increased solar radiation during the day, and there is an increase in temperature with poleward versus equatorward winds. Therefore the associations shown in this paper are consistent with the physical processes known to be operating.

[48] The delayed warming in the tropical Indian and Atlantic Oceans is also a result of changes in atmospheric circulation [*Wallace et al.*, 1998; *Klein et al.*, 1999]. In the Atlantic the relationship of $\nabla \cdot \mathbf{F_A}$ (Figure 11) with local SST anomalies is opposite to that in the Pacific, showing warming of the Atlantic from the changes in the atmosphere heat budget during El Niño. In the tropical Indian Ocean, however, especially in the western part, the results are more like those in the Pacific. This suggests that the changes in surface wind stress are responsible for much of the surface temperature changes, but a feedback and forcing of the atmosphere arises through local convection changes. It was especially noticeable in 1997–1998, although claims have been made of independence from ENSO [*Webster et al.*, 1999; *Saji et al.*, 1999].

[49] These results highlight the fact that over most of the globe away from the tropical Pacific, it is the persistent change in atmospheric circulation driven from the Pacific that results in the changes in surface temperature.

4.3. Individual Events

[50] To reveal how the correlations presented in the previous figures have eventuated from individual ENSO events, we have examined the latitude-time Hovmöller diagrams for several quantities (not shown, but see *Wallace et al.* [1998]). While these reveal to some extent how the individual events contribute to the statistical relationships explored earlier, they also show considerable variability from event to event. *Kumar et al.* [2001] explored the evolution of 200-mbar height for the 1997–1998 event in some detail. However, detailed comparisons of the evolution of each event suggest that the timescale is not necessarily fixed and the evolution in some events is stretched out relative to others, making relationships at fixed lags or leads (used here) not necessarily the best way to examine the evolution. Whether external influences such as the effects of volcanic eruptions are a factor in this or whether it relates more to the amplitude of each event and the way

in which transients perhaps trigger and contribute to the development remain outstanding questions.

5. Conclusions

[51] ENSO events contribute to coherent interannual and even decadal fluctuations in the global mean temperature and, as we have shown, the nature of the ENSO contribution is quite complex. Part of it involves the recharge and discharge of heat in the tropical Pacific Ocean. During and following El Niño events the heat from the ocean is redistributed within the tropical Pacific, and much of it is released to the atmosphere, creating local warming. However, a major part of the ocean heat loss is through evaporation, and the heat is realized in the atmosphere as latent heating in precipitation. This diabatic heating drives large-scale atmospheric overturning that influences the response throughout the tropics and subtropics as well as influencing other teleconnections within the extratropics.

[52] The main tool used in this study is correlation and regression analysis that, through least squares fitting, tends to emphasize the larger events. This seems appropriate as it is in those events that the signal is clearly larger than the noise. Moreover, the method properly weights each event (unlike many composite analyses). Although it is possible to use regression to eliminate the linear portion of the global mean temperature signal associated with ENSO, the processes that contribute regionally to the global mean differ considerably, and the linear approach likely leaves an ENSO residual. We have shown here that 0.06°C of the warming from 1950 to 1998 can be accounted for by the increased El Niño phase of ENSO. The lag of global mean temperatures behind N3.4 is 3 months, somewhat less than found in previous studies. In part, this probably relates mostly to the key ENSO index used, as the evolution of ENSO means that greater or lesser lags arise for alternative indices that also vary across the 1976/1977 climate shift.

[53] We have shown how positive correlations of surface temperatures with N3.4 extend from the equatorial region into the subtropics a year later. Results are fairly similar for both 1979–1998 and 1950–1978, and so this pattern also exists for the entire period, without diminution of the correlations, and thus with an enhancement in statistical significance. However, for 1979–1998 the warming in the central equatorial Pacific develops from the west and progresses eastward. In contrast, for 1950–1978 the anomalous warming begins along the coast of South America and spreads westward, as shown by *Rasmusson and Carpenter* [1982]. This difference in evolution continues as the eastern Pacific south of the equator warms during the +4 to +8 months for 1979–1998 but cools from 1950 to 1978.

[54] Over the oceans, there is an evolution from the maximum anomaly in the equatorial Pacific spreading poleward and to the other oceans over several months. Many tropical land areas tend to be warm from 0 to +8 months. This warmth relates to the relatively sunny and dry, or even drought, conditions during El Niño and so is mainly a result of subsidence and changes in cloudiness and atmospheric circulation. Heat from the ocean is mainly important for the tropical heat sources that drive the teleconnections and tropical large-scale overturning. More generally, over land, there is less evidence for delays with increasing latitude, as seen over the ocean, but instead the whole pattern is delayed by 3–4 months. Also, the extension is to slightly higher latitudes at 4–8 months, especially in the Northern Hemisphere over North America from 45°N to 65°N. This fits with work by *Angell* [2000] but indicates that his result is probably biased by the distribution of stations used and that it is not representative of the land and ocean combined. Because the peak in N3.4 tends to occur about November–December and is phase locked to the annual cycle, these results mean that the maximum warmth occurs in the following northern spring and extends well into the summer. The processes involved are discussed in section 4 and are well established in winter and spring [*Trenberth et al.*, 1998].

[55]   OLR is often used as a proxy for precipitation owing to the dominant changes that occur in cloudiness and high cloud tops. However, the algorithms for translating OLR to precipitation do not account for the real effects of surface temperature changes on OLR or of small changes associated with heating of the atmosphere. High SSTs are associated with the atmospheric convergence, deep convection, and thus low OLR, but also with a flux of latent energy into the atmosphere, condensation and heating of the atmosphere, and transport of heat to higher latitudes where it can be radiated to space. This increase in OLR, seen especially in the subtropics, may be interpreted erroneously by precipitation algorithms as less precipitation. Hence, whereas the precipitation amounts should increase when integrated over the domain, they do not appear to, and this is probably incorrect [*Soden*, 2000]. Although we infer that the increase in tropospheric temperature in the tropics, shown in Figure 14, mainly originates from the increase in precipitation and latent heating and the redistribution from overturning and subsidence in the atmosphere, this signature is not present in the Xie-Arkin data set.

[56]   There is no doubt that the subsurface ocean heat content in the Pacific leads the SST and atmospheric changes. However, the much lower lag correlations between N3.4 and temperatures in the Pacific for 1979–1998 versus 1950–1978 suggest differences in evolution, part of which may have been due to the two volcanic eruptions that occurred, with the Pinatubo event in 1991 estimated to cause a global cooling of ∼0.5°C [*Wigley*, 2000]; see, especially, the residual temperature signal in Figure 3. However, the climate shift in 1976/1977 seems to have been a major factor in fundamentally altering the evolution sequence of ENSO events. This suggests that the subsurface ocean evolution since 1980, which has become the paradigm for ENSO, may not be robust across all events and/or that the links between the subsurface and the surface may have changed. Mechanisms for warming in the tropical Pacific depend on a balance of terms within the ocean [*Neelin et al.*, 1998], and this balance may have shifted. For instance, vertical temperature gradients and upwelling in the eastern tropical Pacific play a key role in westward development, while eastward development relies more on east-west temperature gradients and advection in the central tropical Pacific. We noted in Figure 13 how poorly the SSTs were related to the total ocean heat content anomalies outside of the equatorial Pacific and that this will limit the ability of two-layer model oceans, often employed in intermediate models, to simulate ENSO.

[57]   The negative feedback between SST and surface fluxes can be interpreted as showing the importance of the discharge of heat during El Niño events and of the recharge of heat during La Niña events. Relatively clear skies in the central and eastern tropical Pacific allow solar radiation to enter the ocean, apparently offsetting the below normal SSTs, but the heat is carried away by Ekman drift, ocean currents, and adjustments through ocean Rossby and Kelvin waves, and the heat is stored in the western Pacific tropics. This is not simply a rearrangement of the ocean heat, but also a restoration of heat in the ocean. Similarly, during El Niño the loss of heat into the atmosphere, especially through evaporation, is a discharge of the heat content, and both contribute to the life cycle of ENSO. These observations support the picture put forward by *Barnett et al.* [1991] based mainly on model results in which the SST anomalies are created by ocean dynamics and response to wind forcing, and not by local surface fluxes. However, the role of the surface fluxes and the diabatic component of the ENSO cycle should not be underestimated, as it has implications for the role of ENSO in climate.

[58]   An alternative view of the change in evolution of ENSO is one based upon time filtering of the data into interannual and interdecadal timescales [e.g., *Zhang et al.*, 1997; *Mantua et al.*, 1997; *Giese and Carton*, 1999]. Because the patterns of SST on each timescale are not orthogonal and the processes are nonlinear, strong interactions are implied, and results are difficult to interpret.

The reasons why the change in evolution with the 1976/1977 climate shift occurred are quite uncertain but appear to relate to changes in the thermocline [*Guilderson and Schrag*, 1998; *Giese and Carton*, 1999] that could be linked to climate change and global warming [*Trenberth and Hoar*, 1996; *Meehl and Washington*, 1996; *Timmermann et al.*, 1999].

References

An, S.-I., and B. Wang, Interdecadal change in the structure of the ENSO mode and its impact on the ENSO frequency, *J. Clim.*, *13*, 2044–2055, 2000.

Angell, J. K., Tropospheric temperature variations adjusted for El Niño, 1958–1998, *J. Geophys. Res.*, *105*, 11,841–11,849, 2000.

Barnett, T. P., M. Latif, E. Kirk, and E. Roeckner, On ENSO physics, *J. Clim.*, *5*, 487–515, 1991.

Behringer, D. W., M. Ji, and A. Leetmaa, An improved coupled model for ENSO prediction and implications for ocean initialization, I, The ocean data assimilation system, *Mon. Weather Rev.*, *126*, 1013–1021, 1998.

Cane, M. A., and S. E. Zebiak, A theory for El Niño and the Southern Oscillation, *Science*, *228*, 1085–1087, 1985.

Christy, J. R., and R. T. McNider, Satellite greenhouse signal, *Nature*, *367*, 325, 1994.

Dai, A., K. E. Trenberth, and T. R. Karl, Effects of clouds, soil moisture, precipitation and water vapor on diurnal temperature range, *J. Clim.*, *12*, 2451–2473, 1999.

Deser, C., M. A. Alexander, and M. S. Timlin, Upper-ocean thermal variations in the North Pacific during 1970–1991, *J. Clim.*, *9*, 1840–1855, 1996.

Giese, B. S., and J. A. Carton, Interannual and decadal variability in the tropical and midlatitude Pacific Ocean, *J. Clim.*, *12*, 3402–3418, 1999.

Graham, N. E., Decadal-scale climate variability in the tropical and North Pacific during the 1970s and 1980s: Observations and model results, *Clim. Dyn.*, *10*, 135–162, 1994.

Guilderson, T. P., and D. P. Schrag, Abrupt shift in subsurface temperatures in the tropical Pacific associated with changes in El Niño, *Science*, *281*, 240–243, 1998.

Halpert, M. S., and C. F. Ropelewski, Surface temperature patterns associated with the Southern Oscillation, *J. Clim.*, *5*, 577–593, 1992.

Hellerman, S., and M. Rosenstein, Normal monthly wind stress over the world ocean with error estimates, *J. Phys. Oceanogr.*, *13*, 1093–1104, 1983.

Hurrell, J. W., and K. E. Trenberth, Global sea surface temperature analyses: Multiple problems and their implications for climate analysis, modeling and reanalysis, *Bull. Am. Meteorol. Soc.*, *80*, 2661–2678, 1999.

Jin, F., An equatorial ocean recharge paradigm for ENSO, I, Conceptual model, *J. Atmos. Sci.*, *54*, 811–829, 1997.

Jones, P. D., The influence of ENSO on global temperatures, *Clim. Monit.*, *17*, 80–89, 1989.

Klein, S. A., B. J. Soden, and N.-C. Lau, Remote sea surface temperature variations during ENSO: Evidence for a tropical atmospheric bridge, *J. Clim.*, *12*, 917–932, 1999.

Kumar, A., W. Wang, M. P. Hoerling, A. Leetmaa, and M. Ji, The sustained North American warming of 1997 and 1998, *J. Clim.*, *14*, 345–353, 2001.

Kumar, K. K., B. Rajagopalan, and M. A. Cane, On the weakening relationship between the Indian monsoon and ENSO, *Science*, *284*, 2156–2159, 1999.

Mantua, N. J., S. R. Hare, Y. Zhang, J. M. Wallace, and R. C. Francis, A Pacific interdecadal climate oscillation with impacts on salmon production, *Bull. Am. Meteorol. Soc.*, *78*, 1069–1079, 1997.

Meehl, G. A., and W. M. Washington, El Niño-like climate change in a model with increased atmospheric CO_2 concentrations, *Nature*, *382*, 56–60, 1996.

Meinen, C. S., and M. J. McPhaden, Observations of warm water volume changes in the equatorial Pacific and their relationship to El Niño and La Niña, *J. Clim.*, *13*, 3551–3559, 2000.

Neelin, J. D., D. S. Battisti, A. C. Hirst, F.-F. Jin, Y. Wakata, T. Yamagata, and S. E. Zebiak, ENSO theory, *J. Geophys. Res.*, *103*, 14,261–14,290, 1998.

Newell, R. E., and B. C. Weare, Factors governing tropospheric mean temperatures, *Science*, *194*, 1413–1414, 1976.

Oberhuber, J. M., An atlas based on the "COADS" data set: The budgets of heat, buoyancy and turbulent kinetic energy at the surface of the global ocean, *Rep. 15*, 20 pp., Max Planck Inst. fur Meteorologie, Hamburg, Germany, 1998.

Pan, Y. H., and A. H. Oort, Global climate variations connected with sea surface temperature anomalies in the eastern equatorial Pacific Ocean for the 1958–1973 period, *Mon. Weather Rev.*, *111*, 1244–1258, 1983.

Rajagopalan, B., U. Lall, and M. A. Cane, Anomalous ENSO occurrences: An alternative view, *J. Clim.*, *10*, 2351–2357, 1997.

Rasmusson, E. M., and T. H. Carpenter, Variations in tropical sea surface temperature and surface wind fields associated with the Southern Oscillation/El Niño, *Mon. Weather Rev.*, *110*, 354–384, 1982.

Reynolds, R. W., and T. M. Smith, Improved global sea surface temperature analyses using optimum interpolation, *J. Clim.*, *7*, 929–948, 1994.

Saji, N. H., B. N. Goswami, P. N. Vinayachandran, and T. Yamagata, A dipole mode in the tropical Indian Ocean, *Nature*, *401*, 360–363, 1999.

Smith, T. M., Tropical Pacific sea level variations (1948–1998), *J. Clim.*, *13*, 2757–2769, 2000.

Smith, T. M., R. W. Reynolds, R. E. Livezey, and D. C. Stokes, Reconstruction of historical sea surface temperatures using empirical orthogonal functions, *J. Clim.*, *9*, 1403–1420, 1996.

Soden, B. J., The sensitivity of the tropical hydrological cycle to ENSO, *J. Clim.*, *13*, 538–549, 2000.

Suarez, M. J., and P. S. Schopf, A delayed action oscillator for ENSO, *J. Atmos. Sci.*, *45*, 3283–3287, 1988.

Sun, D.-Z., The heat sources and sinks of the 1986–87 El Niño, *J. Clim.*, *13*, 3533–3550, 2000.

Sun, D.-Z., and K. E. Trenberth, Coordinated heat removal from the tropical Pacific during the 1986–87 El Niño, *Geophys. Res. Lett.*, *25*, 2659–2662, 1998.

Timmermann, A., J. M. Oberhuber, A. Bacher, M. Esch, M. Latif, and E. Roeckner, Increased El Niño frequency in a climate model forced by future greenhouse warming, *Nature*, *398*, 694–696, 1999.

Tourre, Y. M., and W. B. White, ENSO signals in global upper-ocean temperature, *J. Phys. Oceanogr.*, *25*, 1317–1332, 1995.

Trenberth, K. E., Signal versus noise in the Southern Oscillation, *Mon. Weather Rev.*, *112*, 326–332, 1984.

Trenberth, K. E., Recent observed interdecadal climate changes in the Northern Hemisphere, *Bull. Am. Meteorol. Soc.*, *71*, 988–993, 1990.

Trenberth, K. E., and C. J. Guillemot, Evaluation of the atmospheric moisture and hydrological cycle in the NCEP/NCAR reanalyses, *Clim. Dyn.*, *14*, 213–231, 1998.

Trenberth, K. E., and T. J. Hoar, The 1990–1995 El Niño–Southern Oscillation event: Longest on record, *Geophys. Res. Lett.*, *23*, 57–60, 1996.

Trenberth, K. E., and T. J. Hoar, El Niño and climate change, *Geophys. Res. Lett.*, *24*, 3057–3060, 1997.

Trenberth, K. E., and J. W. Hurrell, Decadal atmosphere-ocean variations in the Pacific, *Clim. Dyn.*, *9*, 303–319, 1994.

Trenberth, K. E., and J. W. Hurrell, Comment on "The interpretation of short climate records with comments on the North Atlantic and Southern Oscillations" by W. Wunsch, *Bull. Am. Meteorol. Soc.*, *80*, 2721–2722, 1999a.

Trenberth, K. E., and J. W. Hurrell, Reply to comment by B. Rajagopalan et al. on "The interpretation of short climate records with comments on the North Atlantic and Southern Oscillations" by C. Wunsch, *Bull. Am. Meteorol. Soc.*, *80*, 2726–2728, 1999b.

Trenberth, K. E., and A. Solomon, The global heat balance: Heat transports in the atmosphere and ocean, *Clim. Dyn.*, *10*, 107–134, 1994.

Trenberth, K. E., and D. P. Stepaniak, Indices of El Niño evolution, *J. Clim.*, *14*, 1697–1701, 2001.

Trenberth, K. E., G. W. Branstator, D. Karoly, A. Kumar, N.-C. Lau, and C. Ropelewski, Progress during TOGA in understanding and modeling global teleconnections associated with tropical sea surface temperatures, *J. Geophys. Res.*, *103*, 14,291–14,324, 1998.

Trenberth, K. E., J. M. Caron, and D. P. Stepaniak, The atmospheric energy budget and implications for surface fluxes and ocean heat transports, *Clim. Dyn.*, *17*, 259–276, 2001.

Trenberth, K. E., D. P. Stepaniak, and J. M. Caron, Interannual variations in the atmospheric heat budget, *J. Geophys. Res.*, *107*, 10.1029/2000JD000297, in press, 2002.

Urban, F. E., J. E. Cole, and J. T. Overpeck, Modification of tropical Pacific variability by its mean state inferred from a 155-year coral record, *Nature*, *407*, 989–993, 2000.

Waliser, D. E., and W. Zhou, Removing satellite equatorial crossing time biases from the OLR and HRC data sets, *J. Clim.*, *10*, 2125–2146, 1997.

Wallace, J. M., E. M. Rasmusson, T. P. Mitchell, V. E. Kousky, E. S. Sarachik, and H. von Storch, On the structure and evolution of ENSO-related climate variability in the tropical Pacific: Lessons from TOGA, *J. Geophys. Res.*, *103*, 14,241–14,260, 1998.

Wang, B., Interdecadal changes in El Niño onset in the last four decades, *J. Clim.*, *8*, 267–285, 1995.

Webster, P. J., A. M. Moore, J. P. Loschnigg, and R. R. Leben, Coupled ocean-atmosphere dynamics in the Indian Ocean during 1997–98, *Nature*, *401*, 356–360, 1999.

Wigley, T. M. L., ENSO, volcanoes, and record-breaking temperatures, *Geophys. Res. Lett.*, *27*, 4101–4104, 2000.

Wunsch, C., The interpretation of short climate records with comments on the North Atlantic and Southern Oscillations, *Bull. Am. Meteorol. Soc.*, *80*, 245–256, 1999.

Wyrtki, K., Water displacements in the Pacific and the genesis of El Niño cycles, *J. Geophys. Res.*, *90*, 7129–7132, 1985.

Xie, P., and P. A. Arkin, Analyses of global monthly precipitation using gauge observations, satellite estimates, and numerical model predictions, *J. Clim.*, *9*, 840–858, 1996.

Xie, P., and P. A. Arkin, Global precipitation: A 17-year monthly analysis based on gauge observations, satellite estimates and numerical model outputs, *Bull. Am. Meteorol. Soc.*, *78*, 2539–2558, 1997.

Zhang, R.-H., and S. Levitus, Structure and evolution of interannual variability of the tropical Pacific upper ocean temperature, *J. Geophys. Res.*, *101*, 20,501–20,524, 1996.

Zhang, R.-H., and S. Levitus, Interannual variability of the coupled tropical Pacific Ocean-atmosphere system associated with the El Niño Southern Oscillation, *J. Clim.*, *10*, 1312–1330, 1997.

Zhang, Y., J. M. Wallace, and D. S. Battisti, ENSO-like interdecadal variability: 1900-93, *J. Clim.*, *10*, 1004–1020, 1997.

―――――――――

K. E. Trenberth, J. M. Caron, D. P. Stepaniak, and S. Worley, National Center for Atmospheric Research, P.O. Box 3000, Boulder, CO 80305, USA. (trenbert@ncar.ucar.edu; jcaron@ucar.edu; davestep@ucar.edu; worley@ucar.edu)
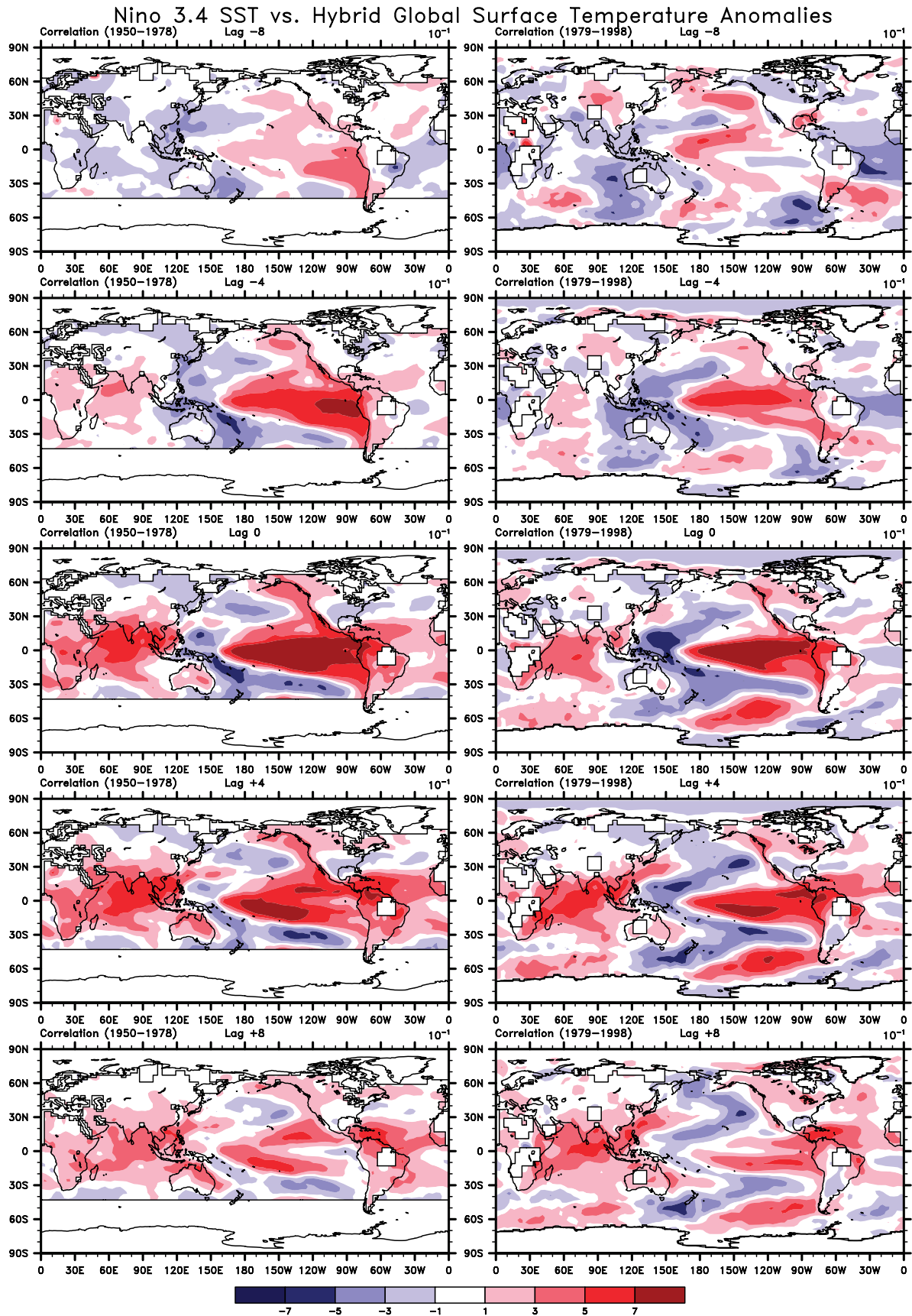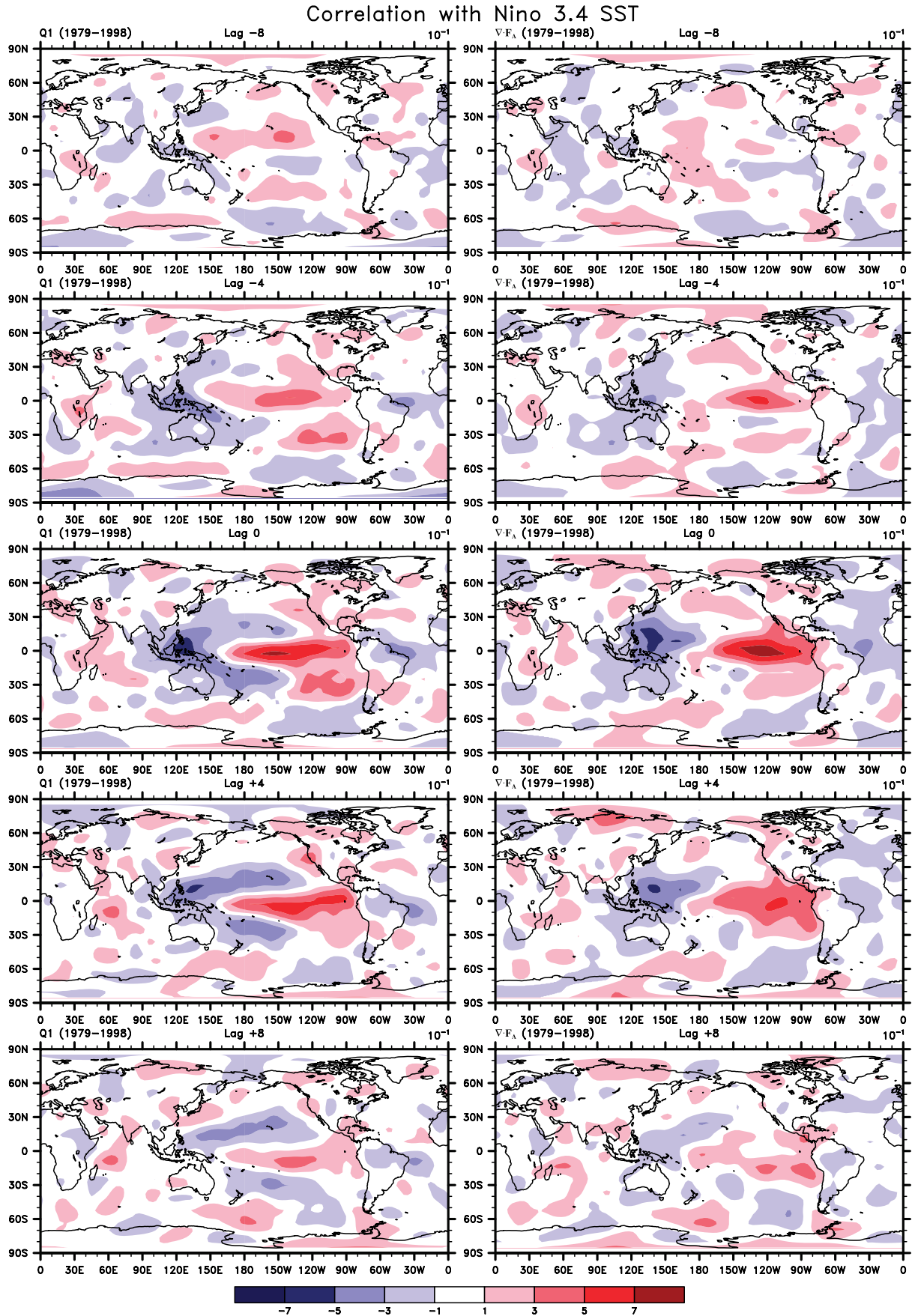
Figure 8. Time sequence of correlations (×10) with N3.4 of surface temperatures (based on the Reynolds SSTs over the ocean blended with the University of East Anglia land data) for (left column) 1950–1978 and (right column) 1979–1998 at −8, −4, 0, 4, and 8 months. Color contour interval is 0.2.
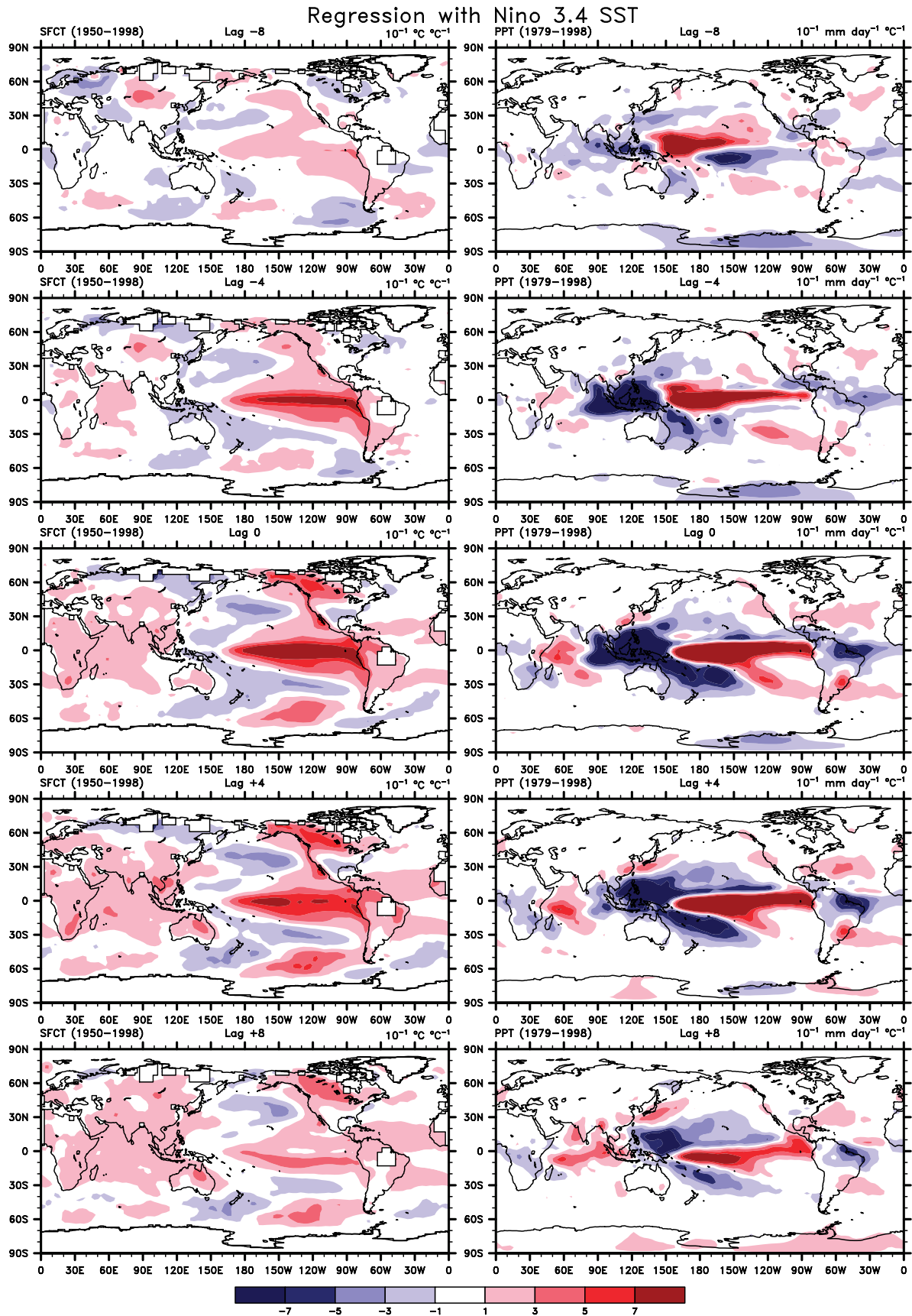
Figure 9. (left) Time sequence of regression coefficients with N3.4, as in Figure 8, but for surface temperatures for 1950–1998 in tenths degrees Celsius and (right) precipitation for 1979–1998 in millimeters per day per N3.4 in degrees Celsius.
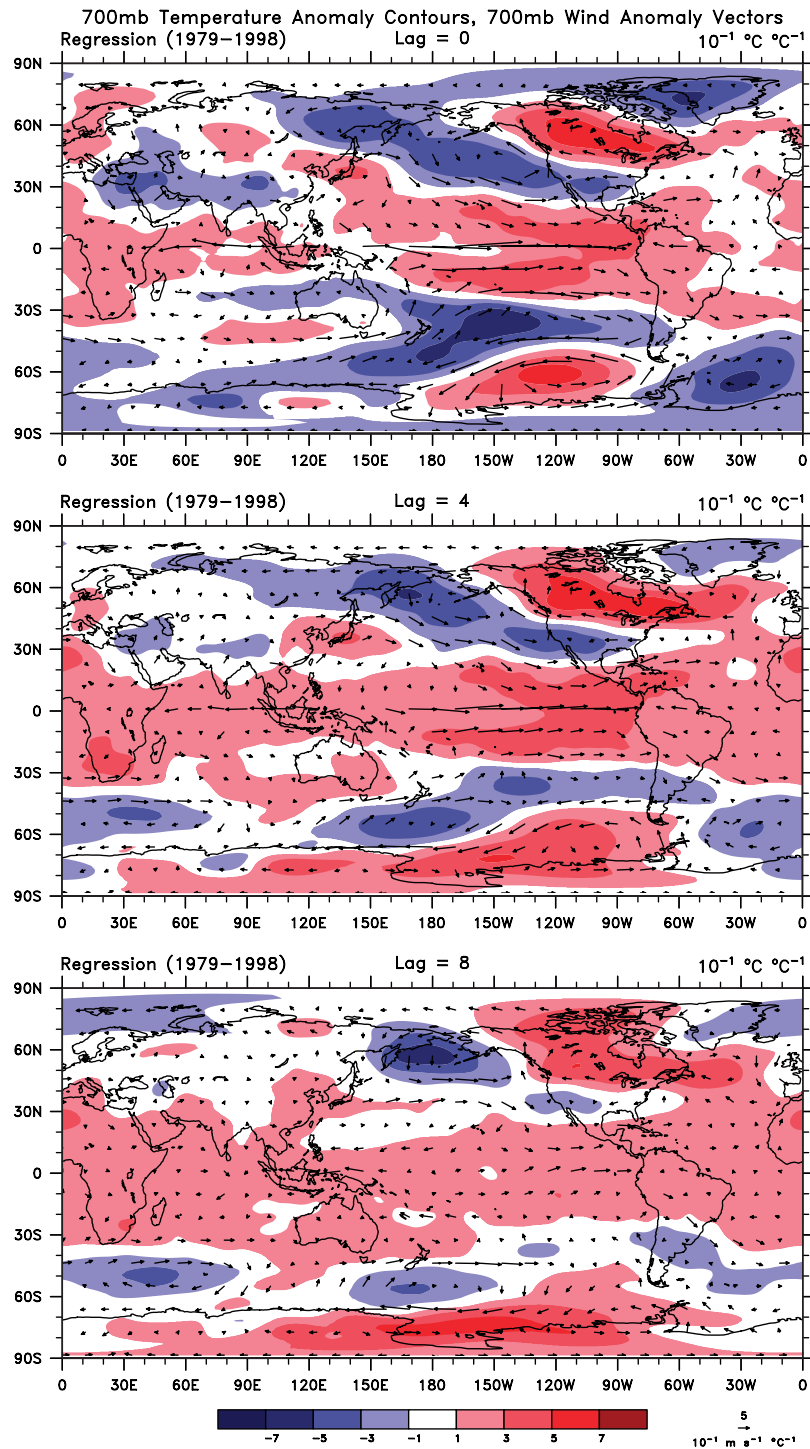
Figure 10. Time sequence of correlations with N3.4, as in Figure 7, but for (left) vertically integrated atmospheric diabatic heating and (right) $\nabla \cdot \mathbf{F_A}$ for 1979–1998.
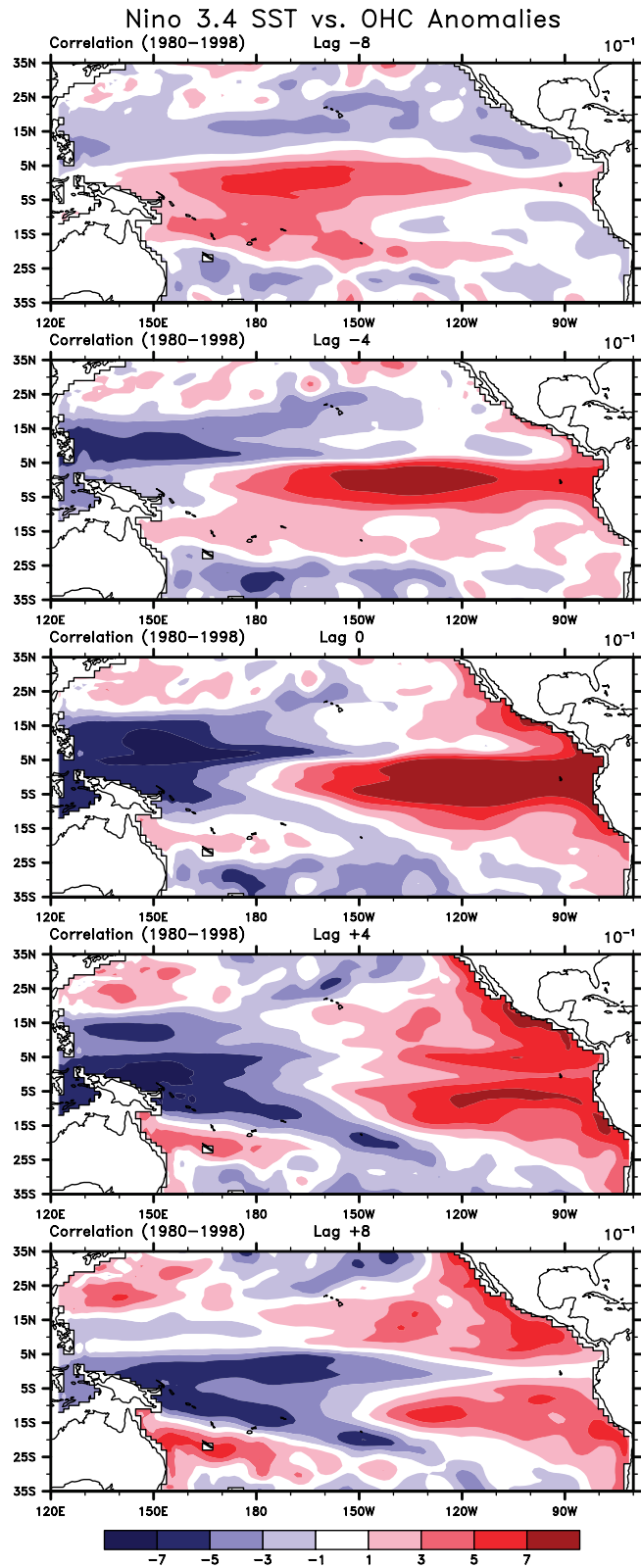
Figure 11. Time sequence of correlations with N3.4, as in Figure 7, but for Pacific Ocean heat content for 1980–1998.

Figure 14. Regression of N3.4 with temperature and vector wind at 700 mbar at 0, 4, and 8 months for 1979–1998. For temperature the units are tenths degrees Celsius per N3.4, and the scale vector wind is given at bottom right.